HYPERSONIC VISCOUS-INVISCID FLOW INTERACTIONS INCLUDING BOUNDARY LAYER SEPARATION ON A FLAT PLATE AT ANGLE OF ATTACK

Thesis by

Gregory D. Hulcher

In Partial Fulfillment of the Requirements

For the Degree of

Aeronautical Engineer

California Institute of Technology

Pasadena, California

1972

(Submitted December 30, 1971)

ACKNOWLEDGEMENTS

I want to express my sincere appreciation to Professor Wilhelm Behrens for his guidance during the course of this research program and to Professors Toshi Kubota and Lester Lees for their interest, suggestions, and support of this effort. I am also grateful to Messrs. P. Baloga, S. Roman, J. Van Dijk, G. Van Halewyn, and H. Mazurowski of the GALCIT Hypersonic Wind Tunnel for their assistance during the experiments; to Mr. G. Carlson and the Staff of the GALCIT Aeronautics Shop for constructing the experimental equipment; to Mrs. Truus Van Harreveld for her assistance in data reduction; and to Mrs. Virginia Conner for her patience during the typing of the manuscript.

In particular, I am addressing this work to my wife, Diane, whose love makes it especially worthwhile.

This work was carried out under the sponsorship and with the financial support of the U. S. Army Research Office and the Advanced Research Projects Agency under Contract DA-31-124-ARO(D)-33, part of Project DEFENDER sponsored by the Advanced Research Projects Agency.

ABSTRACT

Experimental measurements of mean flow properties over the leeward surface and in the near wake of an adiabatic thin flat plate at an angle of attack of $\alpha = 15^{o}$ were obtained at Mach 6 and Reynolds number based on the chord length of 186, 000. The leading edge thickness is the predominant variable which affects the pre-separation interaction region. The effects of the large windward pressure, which separates the boundary layer at $\frac{\ell}{L} \simeq .7$, are felt at points considerably forward of the separation point. The pressure rise in the separation region is similar to the rise on a flat plate-ramp model, and the data correlate according to Chapman's parameters. Also, the leeward side flow of the thin flat plate is found to be very similar to the flow over a wedge whose leeward side is inclined to the same angle. The wake centerline quantities behave similar to those behind a flat plate at zero angle of attack, but the streamwise gradients are less than those behind an inclined wedge. The flow appears to remain laminar throughout the entire field of measurement.

TABLE OF CONTENTS

Table of Contents (Continued)

LIST OF FIGURES

List of Figures (Continued)

List of Figures (Continued)

LIST OF SYMBOLS

a^*	speed of sound at M = 1
C	Chapman-Rubesin factor $(= \frac{\mu_w}{\mu_\infty} \frac{T_\infty}{T_w})$
C_f	coefficient of friction
C_p	coefficient of pressure
D	static pressure probe diameter
h	transverse coordinate at leading edge (Fig. 6)
Kn_t	Knudsen Number based on leading edge thickness
ℓ	coordinate along plate surface (Fig. 3)
L	plate length
M	Mach Number
p	pressure
P_t	total pressure
P_{t_2}, P_p	Pitot pressure
Pr	Prandtl Number
$\vec{q}$	velocity vector
s	shock coordinate (Fig. 6); also distance from forward stagnation point
t	leading edge thickness
T	temperature
U, u	velocity
x	wake streamwise coordinate (Fig. 3)
y	transverse coordinate (Fig. 3)
α	angle of attack
γ	ratio of specific heats for air (= 1.4)

δ boundary layer thickness

ζ vorticity

η, ξ reduced boundary layer coordinates

θ shock inclination

λ molecular mean free path

μ viscosity

ν Prandtl-Meyer expansion angle

ρ density

$\overline{\chi}$ hypersonic viscous-inviscid interaction parameter $(= \frac{M^3\sqrt{C}}{\sqrt{Re_x}})$

$\vec{\omega}$ vorticity vector

Subscripts

b base region

e conditions at boundary layer edge

L based on plate length

m maximum

min minimum

o, r reference conditions

orig conditions which would exist without viscosity

r recovery value

s conditions at shockwave

sp conditions at separation point

t local stagnation quantity

w conditions at the plate surface

oo conditions in freestream

θ shock inclination

$\nu 15$ conditions after 15° Prandtl-Meyer expansion from freestream flow

I. INTRODUCTION

The effects of viscous-inviscid flow interactions on vehicles at high Mach number atmospheric flight are perhaps the most severe and complex for the design engineer. Korkegi[1] has discussed many of these problems and he has provided a helpful bibliography. Most research in high Mach number flows, however, has been concerned with compression surfaces since they produce much greater pressure loads than those produced by expansion surfaces (cf. refs. 2 and 3 for extensive summaries and bibliographies). In contrast to lifting bodies flying at subsonic speeds, where boundary layer interaction and separation on the leeward surface can cause dramatic changes in aerodynamic loads, changes in the flow field on the leeward surface of a hypersonic vehicle have little effect on the net aerodynamic forces. However, even for high Mach number flows over lifting surfaces, Bertram et al[4, 5] and Ferrari[6] have demonstrated the importance of the leeward flow for the attainment of high lift to drag ratios. The problem of viscous-inviscid interaction on the leeward surface of a hypersonic vehicle is important for heat transfer and control effectiveness considerations.

The leeward flow interaction problem, including separation, has been considered theoretically by Klineberg, Kubota, and Lees[7] who calculated the effect of an underexpanded rocket exhaust on the external flow and the flow on the leeward side of a finite length thin flat plate at an angle of attack in viscous hypersonic flow. The results on the flat plate configuration, which is a useful approximation to hypersonic lifting surfaces in high altitude flight, were the primary

motivation for the experiments described herein.

The inviscid shock-expansion model for the flat plate in the experiment predicts a windward-leeward pressure ratio which is greater than 100 (Fig. 1). It was therefore evident that viscosity would play the role of "smoothing out" the large and abrupt changes at the trailing edge of the inviscid model. In addition, the no-slip condition creates a boundary layer which interacts with the inviscid hypersonic flow, especially on the leeward side where the Reynolds number is lower and the Mach number is higher than the freestream values. Therefore, the effects of viscosity create a thick boundary layer with an accompanying subsonic inner layer. The large pressure on the windward side propagates around the trailing edge and forward on the leeward side in the boundary layer, thereby creating a pressure gradient which is adverse to the boundary layer flow. A hypersonic boundary layer over an adiabatic surface, which has relatively little density and momentum, is easily retarded and eventually separated from the surface. The end result is a streamline, pressure, and temperature pattern on the leeward side which is significantly different from the ideal gas model.

Not only is there a stark contrast between the ideal inviscid and viscous gas flow structures, but, as is characteristic of low Reynolds number hypersonic flow, the prominent features of the viscous flow over the leeward side and wake of the thin flat plate are quite sensitive to both freestream conditions and model parameters. Model parameters include incidence to the freestream, leading edge bluntness, and surface temperature. In past publications Bertram,[8]

and Lee[9] have determined the pressures over inclined blunt bodies. Bertram[10] has experimentally combined the effects of leading edge bluntness and viscous effects, while Cheng,[11] Lee,[12], Stollery,[13] and Allegre and Bisch[14] have considered these effects with an additional parameter that includes angle of attack. However, Klineberg's[7] theoretical work is the only one that considers viscous interaction of leeward flow with the windward flow for a body at angle of attack. This problem apparently has not been investigated experimentally.

The objectives of the present experimental study are to investigate (1) the viscous-inviscid flow interactions at Mach number six on the leeward side of a flat plate of two nose-bluntnesses at angle of attack which includes separation of the boundary layer (the angle of attack for onset of separation is about 8^{o}); (2) the high temperature viscous near wake of the flat plate at an angle of attack, and a comparison of these results to those of other configurations such as the flat-plate flow without angle of attack (Batt and Kubota[15]) and the wake of a wedge at an angle of attack (Wu and Behrens[16]).

The experimental techniques and apparatus are described in Part II followed by a description of the data reduction techniques and accuracy estimates in Part III. The presentation and discussion of the results are given in Part IV and a summary of the conclusions is presented in Part V.

II. EXPERIMENTAL APPARATUS AND TECHNIQUES

II. 1. GALCIT Hypersonic Wind Tunnel

The entire experiment was performed in Leg 1 of the GALCIT Hypersonic Wind Tunnel. This facility is a continuous flow, closed return wind tunnel with a 5 in. x 5 in. test section. The Mach number ranges from M = 6.10 for a reservoir pressure of $P_{t\infty}$ = 10 psig to M = 6.14 for $P_{t\infty}$ = 90 psig. The corresponding test section Reynolds number ranges from Re/in. = 46, 000 to 186, 000. The largest pressure was used for the majority of the measurements in this experimental investigation. The air was dried and heated to 275°F to prevent condensation, and a dew point of -40°F was maintained (the specific humidity was smaller than 5×10^{-5}). The tunnel was warmed up sufficiently before any measurements were taken.

The various models used in this experiment were placed at the center of the third port which was 23 in. downstream of the nozzle throat.

II. 2. Models

Three .016 in. thick stainless steel flat plate models, which spanned the entire test section, were used for the tests. The first was 1.0 in. long with the windward side beveled 4° to a moderate bluntness of approximately .003 in. (Fig. 2). A quantitative meaning for the word bluntness will be discussed in Part IV. A second model was beveled in a similar fashion to .004 in. at one end and .005 in. at the other end, so that the resulting total length was 0.954 in. The third model was identical to the second except that five pressure taps were placed spanwise .05 in. apart and 0.4 in. from the .0005 in.

leading edge on the leeward side. Flat tubing ran along the windward side from the orifices and through the tunnel wall. At all times, the models were supported in tension to prevent any dihedral effects (Fig. 2).

With the model securely fastened to the round ports on each side of the tunnel, the two ports were rotated simultaneously through the desired angle with respect to the flow direction which was assumed to be parallel with the test section centerline. Sealed brass "bell jars" were then placed over the model clamps on each port as the test section was evacuated to prevent any leakage through the clamp device.

II. 3. Experimental Measurements

Four kinds of measurements were made on and above the leeward surface and in the near wake of the flat plate model: (1) static pressure, (2) Pitot (impact) pressure, (3) mean hot-wire, and (4) oil film flow visualization.

II. 3. a. Static Pressure

To measure the static pressure, a conventional cone-cylinder static pressure probe with a .042 in. outer diameter and 20° cone tip was used. Four .016 in. diameter orifices were located .08 in. from the probe shoulder. For surface measurements, the probe was bent a few degrees less than the plate incidence to the freestream and then easily forced, by adjusting the probe support actuator, to lie flat on the plate surface so that the center of the orifices were at the desired distance from the leading edge (Fig. 3). A calibration of the reliability of this method is described in Section III. 2. For measurements in the center of the viscous wake, the probe was straightened to be

parallel with the freestream.

Static pressures as low as 0.7 mm. of Hg were experienced on the leeward side of the model for an incidence of 15° and with the highest reservoir pressure (90 psig). Therefore, it was imperative that all joints be carefully sealed with vacuum grease to prevent leakage. A silicone micromanometer, for which the reference pressure was maintained at about a half micron of mercury, was used for the measurements.

II. 3. b. Pitot Pressure

Pitot pressure about the model was measured with probes which were made of stainless steel hypodermic tubing flattened at one end to openings of .010 X .05 in. and .003 X .05 in. The pressure was converted to a voltage by calibrating 5 psi and 10 psi Statham absolute-pressure transducers. The voltages were then amplified and recorded on a Moseley autograph against probe position given by a Helipot potentiometer connected to the probe actuator. All traces with the Pitot probe were taken in a direction normal to the freestream and slow enough to allow for any time lag. Position with respect to the model was established by electrical contact.

II. 3. c. Mean Hot-wire

The mean hot-wire data were obtained with a .0005 in. diameter platinum-10% rhodium wire approximately .05 in. long and soldered between two long and narrow brass needles which were insulated from each other. A constant current of 5 ma., which resulted in a very small overheat so that the temperature of the wire closely corresponded to the total temperature of the flow, was used to

measure the resistance of the wire. A redundant bucking voltage was placed in series with the wire voltage and the net output was amplified and displayed on the Moseley autograph. The method of taking traces with the hot-wire probe was similar to that used for the Pitot probe. The hot-wire probe was determined to be on the model when the wire between the brass needles was short-circuited by the metal surface.

II. 3. d. Flow Visualization

Before the flow field about the flat plate at an incidence was examined in detail, boundary layer separation on the leeward side was observed for various angles of attack by setting the plate at some desired incidence with a thin coat of medium weight oil on the surface. Flow was started in the tunnel and in a short time ($\sim$ 1 minute), a ridge of oil formed in the region of reversed flow, and its location could be determined with scales on the model end plates. Obviously, some error is inherent in this method of measurement, and the separation point could be located to within, at best, 5% of the plate chord length.

III. ACCURACY ESTIMATES AND DATA REDUCTION

III. 1. Model--Wind Tunnel Wall-Interaction

The credibility of the measured data in this experiment depends on first, the two-dimensionality of the flow in the regions of interest, and second, but not necessarily independent from the first, the interaction between the model and the tunnel wall and the probes.

To test the need for fences, which are commonly used to minimize wind tunnel wall effects, sharp fins, or side plates, which were sufficiently large to contain the separation interaction region, were placed 3/4 in. from each tunnel wall. After some near wake Pitot pressure traces and surface static pressures were taken, the fences were carefully removed so as not to change the model itself in any way, and the measurements were repeated. It was found that the fence and non-fence results agreed well within the limits of this experiment.

Disturbances created by the interaction of the model flow and wind tunnel boundary layer did not affect the center line flow for several inches behind the model and therefore near wake measurements were not jeopardized by reflecting shockwaves or the interaction with the side wall boundary layers.

III. 2. Static Pressure

As mentioned previously, very low pressures result from expansions from hypersonic wind tunnel freestream conditions. (The freestream pressure at $P_{t\infty}$ = 90 psig is $p_\infty \cong 3$ mm Hg.) Extreme caution was taken to minimize outgassing and leakage. Before any measurements were taken, the system was evacuated for several

days, or until no pressure reading could be attributed to outgassing. Also, the system remained evacuated when not in use. There were as few junctions as possible and they were carefully sealed.

In this experiment, the conventional static pressure probe was used in an unconventional way to measure the surface pressure distribution. The usual pressure orifices on the surface were not practical because of the small thickness of the "knife blade" flat plate model. Therefore, an extensive and careful calibration of the technique described in Section II. 3.a was carried out.

First, the model was set parallel to the freestream, and the surface pressure was measured with various "sliding" probes and the results were compared to pressure given by weak viscous-inviscid interaction theory in Fig. 4. The .042 in. O.D. sliding probe was selected for the experiment and further calibration because the response time was much less than for the narrower probes, and also because the increased size did not seem to give significantly less reliable data.

The .042 in. O.D. sliding probe was calibrated further by installing a long (6 in.), $\frac{1}{2}$ in. thick sharp edged flat plate into the tunnel. Pressure orifices were located at several distances from the leading edge, and pressure leads ran to a manifold connected to the silicone micromanometer. This plate could be inclined up to 10^{o} expansion over the tapped surface before blockage prevented proper tunnel flow. Pressures were then compared on this surface with and without the sliding probe lying directly on the pressure taps. The data showed that the static pressure, as measured by the surface taps,

was consistantly higher with the probe present. The increase averaged about 3 percent, and was not greater than 4 percent. These measurements were made from 1.4 in. to 1.6 in. from the leading edge.

A second calibration consisted of placing the sliding probe on the L = 1 in. plate described earlier with pressure taps at $\ell/L = .4$ and $\alpha = 15^{o}$.

When the probe was placed on the surface, the surface tap and probe simultaneously measured a 7 percent increase in pressure over that measured by the surface tap without the probe present. Moreover, the pressure indicated by the sliding probe remained essentially constant as the probe was raised at least one probe diameter above the plate surface.

Although this calibration was obtained at only one station on the plate, the results are encouraging insofar as this conventional cone-cylinder static pressure probe can reliably measure the surface pressure distribution. It should be emphasized that this technique will fail in stagnation regions and in general where the direction of flow is not parallel to the probe axis.

Static pressure probes are sensitive to misalignment. Therefore, careful consideration of this error must be given in the near wake, especially in the separation region. Igawa[17] found that the 4 hole probe was insensitive to a misalignment of up to 5^{o}. It was therefore felt that the measurements were reliable with the possible exception of near the trailing edge.

One final possible error in static pressure measurements is that resulting from hypersonic viscous interaction on the probe which has been measured by Behrens.[18] However, in this experiment, all of the static pressure data were taken in regions of low Mach number so that this correction was negligible.

III. 3. Pitot Pressure

The Pitot pressure field, even in the absence of any other kind of experimental data, can yield much information about the general hypersonic flow construction. Some important errors, however, must be considered: (1) misalignment, (2) streamline displacement, (3) the interaction between shock waves and the strong shock ahead of the probe, (4) the finite size of the Pitot probe opening, and (5) low Reynolds number, or viscous effects.

McCarthy[19] found less than a three percent error for up to 17^{o} of Pitot probe misalignment in the near wake of a cylinder in hypersonic flow. Therefore, Pitot data were considered erroneous, with respect to misalignment, only in the separation, or recirculation, region.

The error due to the streamline displacement by a Pitot probe can be significant if one wants to determine, say, the dimension of location of a boundary layer or shear layer. The near wake viscous region in this experiment was at least ten times wider than the height of the probe front, so this error was of little concern in the wake. Within the boundary layer, displacement effects can be more sensitive to the ratio of probe height to boundary layer thickness, and so even though this ratio was greater than ten, for the detailed boundary

layer measurements, the hot-wire was used as an alternative means of defining the boundary layer thickness.

The shock waves in the flow were located at the halfway point in the Pitot pressure jump (Fig. 5). Shockwave interaction with the probe can diminish the magnitude of the jump as well as change slightly its location. Therefore, the Pitot traces were faired into what would be closer to an ideal jump trace (Fig. 5). The change in shock location has been estimated to be a small fraction of the probe height[20] and is therefore negligible.

When the Pitot probe was on the model surface, it measured a pressure which was about twice the surface static pressure. This was caused by the finite probe height ($\approx .005$ in.) and low Reynolds number effects, and the result was a measured Mach number of about one at the surface. It was possible, however, to make a correction for the data at stations on the model where the boundary layer is not in a region of a positive, or adverse, pressure gradient. It will be shown later this region includes $\ell/L \leq .5$ in the present experiment. The methods of data reduction and correction are described in the next section (III. 4).

Finally, the very low density portions of the hypersonic boundary layer in this experiment mean that the Reynolds number based on the Pitot probe height can be small enough to introduce viscous and rarefaction effects which can cause the measured Pitot pressure to differ significantly from the idealized value. Although Ramaswamy[21] has outlined the corrections which can be incorporated into the data reduction procedure, this correction was not used since

the revision of data mentioned in the last paragraph, and which is described in detail in the next section, already compensates for this low Reynolds number error.

III. 4. Data Reduction Procedure

Although knowledge of the Pitot pressure field alone about the model can show the general characteristics of the flow, a detailed reduction to all flow parameters was desired over the leeward surface, and before separation in particular. This required that at least three independent parameters be known in the region where viscous effects are important, namely the Pitot pressure, static pressure, and total temperature. In the inviscid field, one can completely determine the flow field when given the total temperature (which remains equal to the freestream total temperature), Pitot pressure, and the shape of the shock wave through which the streamlines in the inviscid flow have passed.

The regions of study for this adiabatic flat plate at an incidence can be divided into three regions: (1) the combination of the boundary layer prior to separation and the inviscid flow between this boundary layer and bow shock (the distinction between these will be discussed later); (2) the separated, or recirculation, zone; and (3) the near wake.

Figure 6 gives a schematic diagram of the first region along with the nomenclature used in reducing the data. To calculate the flow parameters in the viscous region bordered by the dashed line in Fig. 6, the static pressure which was measured on the model surface was assumed to be the same through the entire boundary layer. Since

Pitot pressure was known, only an estimate of the total temperature had to be made. This was done with the mean hot-wire measurements.

The boundary layer hot-wire traces served two purposes: to establish the total enthalpy distribution, and to help identify the boundary layer edge when not possible with Pitot pressure profiles. The form of the total temperature distribution could be found by measuring the variation of the resistance of the wire (Section II. 3. c.) which has a minimum at the model surface (corresponding to the recovery temperature) and a maximum at $y \simeq .9\,\delta$ according to the similarity solution for Pr = . 72 and a range of edge Mach numbers comparable to those in this experiment. Figure 7 shows some normalized hot-wire traces, compared to the constant-pressure similarity solution. For purposes of data reduction, it was assumed that the wall temperature was the recovery temperature of a flat plate,

$$T_r \cong T_e \left(1 + \frac{\gamma-1}{2} M_e^2 \sqrt{P_r}\right) = T_{t\infty} \frac{\left(1 + \frac{\gamma-1}{2} M_e^2 \sqrt{P_r}\right)}{\left(1 + \frac{\gamma-1}{2} M_e^2\right)}$$

To determine the edge of the boundary layer, the maximum total temperature in a similar compressible boundary layer of constant pressure with M = 4. 0 occurs at $y = .89\,\delta$ (Fig. 8). Therefore, the hot-wire voltage peak values were used as a guide to define δ as shown in Fig. 7. The fact that all of the hot-wire traces have approximately the same form as the similarity profile (Fig. 7) means that this technique is quite reliable.

Part IV presents some hot-wire traces to show how the total temperature distribution differs in regions of adverse pressure

gradient and boundary layer separation.

Finally, correction for the non-zero velocity at the model surface, which was mentioned in Section III. 3., had to be made. Figure 9 shows the measured velocity at $\ell/L = .254$ which is typical of the pre-separation boundary layer data. This type of error has also been confronted in experiments by Korkegi[22] and Kendall.[20] Korkegi had measured the skin friction which provided a velocity gradient at the surface so that an accurate fairing of the velocity profile could be made. Kendall did not have this gradient available, but he was also able to fair the velocity profile to zero at the wall on the basis of the near linear dependence of velocity on distance from the wall. This latter technique was also employed to adjust the data in this experiment (Fig. 9) since it was felt that this part of the boundary layer was not significantly affected by the separation or adverse pressure gradient. The other flow quantities were adjusted accordingly in the region where the faired velocity curve departed from the measured values.

The inviscid rotational flow above the boundary layer may be calculated, knowing the shock shape and the Pitot pressure. In order to calculate this inviscid flow, mass conservation gives (Fig. 6)

$$\rho u dy = \rho_\infty u_\infty dh$$

where ρ and u are averaged over the infinitesimal distance dy. Rewriting:

$$\frac{dh}{dy} = \frac{\rho_\infty u_\infty}{\rho u} = \frac{\rho_\infty u_\infty}{\rho_{t\infty} a^*} \quad \frac{1}{(u/a^*)(\rho/\rho_{t\infty})}$$

Now since, for inviscid or ideal gas flow, $T_t = T_{t\infty}$, then

$$\frac{P_t}{P_{t\infty}} = \frac{\rho_t}{\rho_{t\infty}}$$

Therefore

$$\frac{dh}{dy} = \frac{\rho_\infty u_\infty}{\rho_{t\infty} a^*} \frac{1}{\left[\frac{u}{a^*}(M)\right]\left[\frac{\rho}{\rho_t}(M)\right]\left[\frac{P_t}{P_{t\infty}}\right]}$$

where

$$M = M(P_p/P_t)$$

The total pressure can be determined as a function of h by knowing the shock inclination where the streamline crosses, and $P_p(y)$ is obtained from the measurements. Integration is initiated at the shock ($y = y_s$) at which point everything is known about the flow just behind the oblique bow shock. At each step of the integration, all parameters in the inviscid flow could be calculated since M, P_t, and T_t were known.

An accurate expression for the bow shock inclination as a function of h (Fig. 6) is crucial for the correct computation of the inviscid flow field. The following method was used to determine a power law expression for the shock shape

$$S = Ah^B .$$

The result was verified by a few shock position measurements with the hot-wire.

As mentioned before, flow near the plate surface was determined by combining the Pitot pressure with the surface static pressure, which is assumed to be constant with y, through a distance above the surface, which is at least the boundary layer thickness. At the point $y = \delta$, where it was still assumed that $p = p_w$, and where it was also assumed that the streamline there had not suffered any total pressure loss (i.e., the streamline was just entering the boundary layer), one could calculate the mass flow between $y = 0$ and $y = \delta$ to determine at which point h the streamline crossed the shock (Fig. 6). In addition, the shock inclination to the freestream at this point could be calculated by knowing the ratio $P_t/P_{t\infty}$ which remains constant along a streamline until it enters the dissipation region of the boundary layer.

The shock location and slope were also calculated at a second point according to the detailed Pitot pressure profile at $\ell/L = .254$ for each configuration. Figure 10 shows the relation of the Pitot pressure jump with shock angle at a freestream Mach number of 6.14. Since practically all of the streamlines in the inviscid region of interest pass through a shock wave of no more than 30° inclination to the freestream, the shock angle is in a range not too sensitive to error in the Pitot pressure jump. To illustrate this for a shock inclination of 15°, a ten percent error in the Pitot pressure jump results in a ten percent error in shock angle, five percent error in M_s, and a six percent error in total pressure ratio across the shock wave. However, for streamlines nearer to the boundary layer edge, the shock angle with respect to the freestream direction is

considerably greater ($\theta > 30^{o}$) so that the use of a Pitot pressure jump to determine shock angle is practically futile. This is why the method of determining the total pressure jump for a specific streamline (Fig. 5) entering the boundary layer was used to help establish a bow shock shape.

These data from two points on the shock were sufficient to determine the constants A and B in the power law curve fit to the shock shape.

IV. RESULTS AND DISCUSSION

The first section of this part presents a general description of the flowfield and pressure distribution about the flat plate at an incidence as obtained with the flow visualization, Pitot pressure, mean hot-wire, and static pressure surveys. Most of these results are for $\alpha = 15^{o}$. Sections 2, 3, and 4 consider the general flow field as divided into three regions. The first is the interaction region near the leading edge where emphasis is placed on the effects of tip bluntness and a definition of the flow quantities within the entropy and boundary layers. The second region is the separated flow region and will be discussed in Section IV. 3. The final section (Section 4) considers the near wake.

IV. 1. Flow Field Description and Static Pressure Distribution

Flow Field

The Pitot pressure survey, which is shown in Fig. 11 a, b, provides a clear picture of the flowfield structure on the leeward surface and in the near wake of the thin flat plate at an incidence. The probe was moved from its starting position in a direction normal to the freestream. Shown are traces at intervals of $\Delta(\ell/L) = .1$ over the surface, and traces at stations in the near wake to illustrate the main features of the flow. As evidenced by the large pressure jump, the bow shock is quite strong even though it has interacted with the following expansion. The compression of the flow above the point of separation ($(\ell/L)_{sp} \approx .75$) and recirculation bubble is shown by the gradual shock formation at the stations $\ell/L = .8$, .9, and 1.0. This separation shock coalesces with the upper wake shock at $x/L = .45$ for $\alpha = 15^{o}$

(x = 0 at the trailing edge).

A conspicuous feature of the Pitot pressure distributions in Fig. 11a is the lack of distinction between a viscous boundary layer and inviscid region above the leeward surface prior to separation. In other words, the conventional method of measuring a boundary layer thickness with Pitot pressure traces used by Kendall[20] and others cannot be used here because of the strong entropy gradient normal to the streamlines which have passed through the highly curved bow shock wave near the leading edge. Therefore, part of the boundary layer edge was determined with the aid of hot-wire traces described in Section III.4.

The flow field descriptions for $\alpha = 15^{\circ}$ and 22° from the combined Pitot and hot-wire data are shown in Figs. 12 and 13. In these figures the solid lines represent shock waves and the dashed lines bound the viscous regions which were determined as shown in Fig. 4. The contrast between the experimental flowfields diagrammed in these figures and the shock-expansion model in Fig. 1 demonstrates the importance of the present research effort.

Static Pressure on the Leeward Surface and in the Wake

The leeward surface and near wake static pressure for the t = .003 in. flat plate at $\alpha = 15^{\circ}$ incidence is compared in Fig. 14 to the simple inviscid pressure calculation shown in the introduction which is calculated by ignoring bluntness and the viscous boundary layer. After a large jump in the bow shock the pressure along the surface quickly decreases to a minimum at $\ell/L = .55$ and rises again due to the propagation of pressure upstream through the subsonic portion of the viscous layer, which has induced the boundary layer to

separate at $\ell_{sp}/L = .75$. Also shown in Fig. 14 is the result from the integral theory of Klineberg, Kubota, and Lees[7] at a Reynolds number about 2.5 times that of the measurement which qualitatively predicts the behavior of the pressure distribution even though the effect of leading edge bluntness and the boundary layer flow on the windward side are not taken into account properly. With the knowledge gained through this experimental investigation, it appears possible to modify this integral theory and predict this type of flow more accurately.

Division of Flowfield into Three Regions

The leeward surface and wake static pressure field for the adiabatic thin flat plate at an incidence, as shown in Fig. 14 can be divided into three regions which roughly coincide with the regions described in Section IV.1: 1) $0 < \ell/L \leq .5$, where the boundary layer is still attached, although there is interaction with the inviscid, but rotational, flow in the rest of the shock layer; 2) $.5 < \ell/L < 1.0$, which includes the partial recovery of pressure due to diffusion forward from the trailing edge (this region will also be referred to as the "free interaction" region); and 3) the near wake region ($x/L > 0$), in which the pressure recovers to and slightly overshoots the free-stream value.

There is, of course, no fine dividing line where one effect takes over and another effect seizes to influence the flow.

IV.2. Interaction Region Near the Leading Edge

Although the separated flow on the leeward side of the flat plate at an incidence is the predominant feature with regard to practical considerations such as pressure distribution and heat transfer, a

thorough understanding of the region which includes the attached boundary layer and, in fact, the entire shock layer is necessary to analyze the flow field over the entire leeward surface. In view of the literature cited in the introduction, it was felt that the effects of bluntness should also be examined directly because to reduce the nose heat transfer for hypersonic vehicles, the curvature must be reduced.

It should be emphasized here that for the freestream Reynolds numbers in this experiment (Re_∞/in. = 186, 000), a possibility of rarefaction effects exist for small characteristic lengths. Based on the leading edge thickness, the freestream Knudsen number, λ_∞/t, for t = .0005 in. is Kn_t = .1 while Kn_t = .012 for t = .004 in. Therefore, only in the immediate region of the sharp leading edge can there exist any experimental error due to the assumptions of continuum flow, and certainly, all of the measurements in the present experiment are outside of this error region.

Static Pressure on the Flat Plate Leeward Surface

Both viscous and bluntness effects contribute an increase in pressure over the ideal Prandtl-Meyer expansion value, $p_{\nu 15}$. To see the relative magnitudes of these two effects experimentally, the measured pressure distributions on the leeward surface for nose bluntnesses of t = .0005 in. and t = .004 in. are plotted in Fig. 15. As the Reynolds number based on the leading edge thickness and freestream conditions is increased from 95 to 750, the minimum pressure, which is followed by the separation interaction, increased from

$(p/p_\infty)_{min.}$ = .245 to .305. From a practical standpoint, this small addition to the bluntness does little to alleviate nose heat transfer, yet the pressure in the leading edge interaction region is increased significantly.

Cheng et al[11] have theoretically calculated the pressure over an ideally sharp semi-infinite plate at an angle of attack in viscous hypersonic flow and also over a blunt plate in inviscid flow.* In both cases, the present experimental values were larger than Cheng predicted which indicates that the two effects have to be combined for a more accurate theoretical prediction. Cheng's theory, however, is based on hypersonic small disturbance approximations and also limited to $\gamma - 1 \ll 1$. The conditions of this experiment only marginally meet these qualifications.

Three simple flow models were therefore examined which would be appropriate for the present configuration and which will give more insight into the physical phenomena occurring near the leading edge. These models take into consideration viscous interaction effect and bluntness.

1. Viscous-Inviscid Interaction Model for Flow over Sharp Plate

This approach, which bypasses any effect of the leading edge bluntness, uses hypersonic viscous-inviscid interaction theory[23] based on the inviscid leeward side flow conditions obtained by Prandtl-Meyer expansion as described in Fig. 1. The surface pressure calculated by this technique (Fig. 15) is substantial relative to the inviscid value (e.g. $\chi_{\nu 15} = 6.19$ and $p/p_{\nu 15} = 3.93$ at $\ell/L = .3$), but it does not account entirely for the value measured, even for the sharp edged plate.

* Cheng's pressure distribution calculations did not combine angle of attack, bluntness, and boundary layer effects simultaneously.

It is concluded that leading edge bluntness plays an important role in the actual flow.

2. Inviscid Model for Flow Over a Blunt Slender Body

The second approach, which shows the influence of a hemi-cylindrical nose on an inviscid flow over the leeward side, is described in detail in Appendix A. This model employs a semi-empirical method based on the blast wave solution as used by Lee.[12] This predicts quite accurately the pressure distribution when bluntness effects predominate viscous effects. However, the results of this calculation also are low compared to the measured pressures.

3. Model of Viscous-Inviscid Flow Interaction on Blunt Nosed Plate

The real flow situation, as observed in this experiment, is a combination of the two effects just described. Appendix A also shows a simplified, but convenient way in which the inviscid flow field over the blunt model described in the last paragraph can be used to calculate an additional pressure induced by a "local" viscous-inviscid interaction. For example, at $\ell/L = .254$, $\bar{\chi}_{orig} = 2.31$ and $p/p_{orig} = 1.95$ for $t = .0005$ in., and $\bar{\chi}_{orig} = 2.9$ and $p/p_{orig} = 2.35$ for $t = .004$ in. The results from this calculation compare more favorably to the measured pressures (Fig. 16). Based on these results, viscous and bluntness effects contribute roughly equally to the surface pressure of the sharp plate while bluntness is more predominant in the leading interaction region of the blunt plate.

It should be noted that size limitations allowed only pressure measurements starting at $\ell/L \simeq 0.25$. For both the sharp and blunt

models, the pressure dropped approximately as $\ell^{-\frac{1}{4}}$. Inasmuch as $p \sim \ell^{-\frac{1}{2}}$ in purely viscous-inviscid interaction (Fig. 15) and $p \sim \ell^{-\frac{2}{3}}$ (Appendix A), it appears that the effect of the windward pressure is making itself felt considerably closer to the leading edge than where the boundary layer actually separates. It therefore seems that in addition to the bluntness and viscous effects, the subsonic portion of the hypersonic laminar boundary layer allows the adverse gradient to influence the pressure distribution far into the leading edge interaction region.

Flow Quantities in Shock Layer

To fully understand the effect of leading edge bluntness on the expanding flow over the leeward side of a thin flat plate at an angle of attack, a detailed description of the flow between the plate surface and bow shock prior to boundary layer separation for $\alpha = 15^{o}$ was obtained for t = .0005 in. and t = .004 in. within the limitations stated in the data reduction procedure described in Section III. 4. The freestream conditions remained at $M_{\infty} = 6.14$ and $Re_{\infty}/in. = 186,000$.

It is shown in the previous results that a small degree of bluntness (t/L still << 1) can profoundly affect the hypersonic flow on the leeward, or expansion side, of a flat plate at an incidence. This is further evidenced by comparing a Pitot pressure profile for each bluntness in Fig. 17. In this figure, the distinction between a boundary layer and inviscid region becomes clear for the sharp leading edge which confirms the conclusion that streamlines entering the boundary layer "far" downstream from the nose have passed through a strong

and highly curved shock close to the blunt leading edge. The bow shock strength has lessened considerably for the sharp edge.

Using the techniques described in Section III. 4, the measured data give various flow parameters throughout the pre-separation region which were calculated on the IBM 360/65 computer at the California Institute of Technology for each leading edge bluntness. They are plotted in the physical plane in Figs. 18 a, b and 19 a, b. The curve fit forms for the bowshock waves were determined to be as follows (note nomenclature in Fig. 6):

Blunt model: t = .004 in.

$h < .0878$:

$$S = 9.282h^{1.486}$$

$h > .0878$:

$$S = 6.0578h - (1.0426h - .0098)^{\frac{1}{2}}$$

Sharp Model: t = .0005 in.

$h < .0643$:

$$S = 8.871h^{1.3055}$$

$h > .0643$:

$$S = 6.0578h - (.3044h + .0013)^{\frac{1}{2}}$$

The curve fits were split into two parts so that the shock would asymptotically approach the freestream Mach line ($\mu_\infty = 9.37^\circ$).

Figures 18a and 19a show Mach number, static pressure, and total pressure profiles for $\ell/L = .254$ and .454; while Figs. 18b and 19b illustrate the mass flux, velocity, and static temperature distributions.

These profiles show that the flow in the layer between the boundary layer and bow shock wave is qualitatively similar to shock layer flow over slender bodies aligned with the freestream hypersonic flow.[20] The expansion which immediately follows the bow shock wave, however, introduces some differences from a body at zero incidence. For example, even though the Mach number decreases when a streamline passes through the shock, there is an increase in M through the expansion so that just outside the boundary layer on the sharp plate the Mach number is about 7.2 at $\ell/L = .454$ (recall that $M_{\nu 15} = 9.5$); while for the blunt plate, the boundary layer edge Mach number hardly exceeds the freestream value ($M_\infty = 6.14$). This brings to attention an important aspect of the properties of streamlines which pass through a curved bow shock and then expand over the leeward surface; a process not present for zero incidence.

When a streamline passes through the bow shock caused by a slightly blunted tip, and then expands over the leeward side of the plate, the trajectory typically follows a path as sketched below:

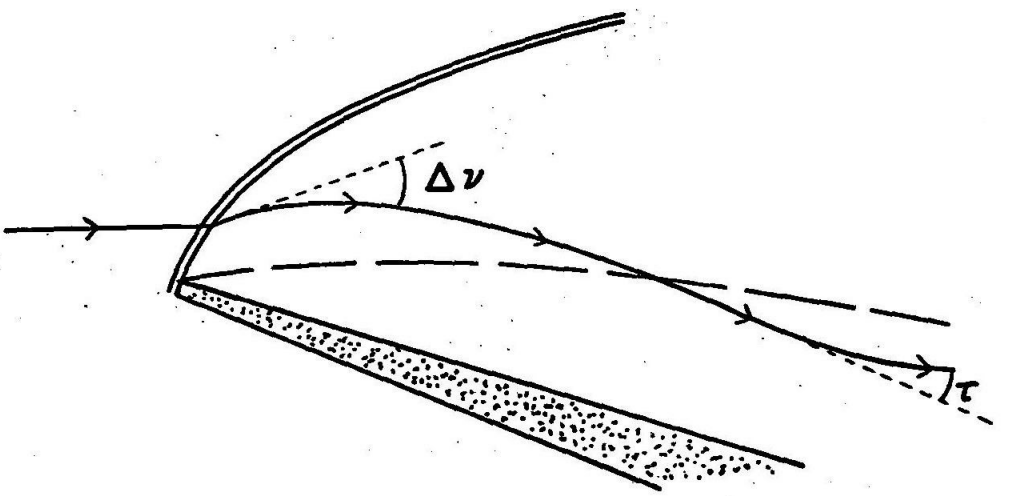

First, the streamline is deflected away from the surface, then an isentropic expansion $\Delta\nu$ followed by displacement τ by the rapidly growing hypersonic boundary layer. It was seen in Part III how the Pitot pressure jump varied with shock inclination to the free-stream (Figure 10). Similarly, the total pressure and Mach number aft of an oblique shock change a great deal with θ as shown in Fig. 20. Therefore, streamlines which have passed through different points of the bow shock differing by only a few degrees of inclination can end up with considerably different Mach numbers after expanding $\Delta\nu$ (Figure 21). For this reason, one would expect a larger Mach number gradient in the rotational inviscid flow above the boundary layer for a thicker leading edge. This fact explains the increase in Mach number gradient at the boundary layer edge for t=. 004 in. (Fig. 19a), while the Mach number is relatively constant above the boundary layer for t = .0005 in. This observation, along with the fact that the total pressure varies considerably, illustrates in part why the flow in the entire shock layer, and particularly the boundary layer flow itself, is so sensitive to the leading edge bluntness. It should be noted, however, that the velocity outside the boundary layer deviates very little from the freestream velocity; i.e. $1 - u/u_\infty \ll 1$ for $y > \delta$.

Vorticity Interaction

A topic which may be important in this problem is the influence of vorticity in the external flow. In fact, if the vorticity in the supposedly inviscid entropy layer is large enough, the shear stress in the outer layer may be so large that the entire shock layer region must be considered viscous. Since the results of the present measurements

show significant flow property gradients above the boundary layer (Figs. 18 and 19), it is necessary to calculate the importance of the vorticity in the outer layer relative to some characteristic boundary layer vorticity.

Hayes and Probstein[23] define the vorticity interaction parameter

$$\Omega = \frac{\zeta_{inv}}{\rho_{inv} u_{inv}} \int_0^{y^*} \rho \, dy$$

where the subscript "inv" denotes conditions at the edge of the equivalent body in the equivalent inviscid flow. For high Mach number flows over adiabatic surfaces where the boundary layer thickness and displacement thickness are nearly equal, it will be sufficient for order of magnitude considerations to equate "inv" conditions with conditions which were measured at the boundary layer edge (i. e. where $u/u_\infty \approx 1$).

Hence take

$$\Omega = \frac{\zeta_e}{\rho_e u_e} \int_0^{y^*} \rho \, dy$$

where y^* is defined by the relation:

$$\eta(\ell, y) \equiv 1 = \frac{u_e}{\sqrt{2\xi}} \int_0^{y^*} \rho_\omega \mu_\omega u_e \, d\ell \quad (u_e \equiv u_\infty)$$

The extreme case for which data are available in this experiment is at $\ell/L = .254$ on the blunt model (t = .004 in.).

To calculate the vorticity outside the boundary layer edge, ζ_e, one can in principle use the experimental velocity distribution. However, much greater accuracy is obtained by the total pressure gradient

using Crocco's Theorem:

$$\vec{q} \times \omega = - T \Delta S$$

where

$$\Delta S \approx \frac{dS}{dy} = - C_p \left(\frac{\gamma-1}{\gamma}\right) \frac{1}{P_t} \frac{dP_t}{dy}$$

Since $\vec{q} \times \vec{\omega} \approx -y \frac{\partial u}{\partial y} \hat{j}$ in the outer layer, then

$$\zeta(y) = \frac{\partial u}{\partial y} \approx - \left(\frac{T_\infty}{u_\infty}\right)\left(\frac{R P_{t\infty}}{P_t(y)}\right)\left(\frac{d}{dy}\left(\frac{P_t(y)}{P_{t\infty}}\right)\right)\left(\frac{T}{T_\infty}(y) \Big/ \frac{u}{u_\infty}(y)\right)$$

which gives

$$\frac{\zeta(y)\delta}{u_\infty} = \frac{\delta}{\gamma M^2(y)} \left(\frac{P_{t\infty}}{P_t(y)}\right) \frac{d}{dy}\left(\frac{P_t(y)}{P_{t\infty}}\right)$$

Substituting values at $y = \delta = .06$ in. into the above parameter,

$$\frac{\zeta_e \delta}{u_\infty} = .078$$

Therefore, at this station, the vorticity interaction parameter $\Omega = .0082$. The interaction parameter values at other stations on either model are less than this value. Hence, for the present experimentally found flowfields, the vorticity interaction is negligible, even though the outer inviscid flow is rotational and has strong lateral entropy gradients.

Boundary Layer Growth

The nature of viscous hypersonic flow, especially on an expansion side of a model, is that the mean density in the boundary layer is very small so that the displacement thickness, δ^*, and boundary

layer thickness, δ, are nearly equal, and therefore a measure of viscous-inviscid interaction is the growth of δ. The boundary layer thickness was found from the Pitot pressure profiles for the sharp leading edge (Fig. 5) and with the aid of the hot-wire profiles, as described in Section III. 4., for the blunter model. The consistency of the two methods was verified at stations where both methods could be used. The results are shown in Fig. 22 along with those obtained by Kendall[20] for the sharp flat plate at zero angle of attack. In view of the assumptions made for the hot-wire profiles and of the fact that two different methods were used to measure the boundary layer thickness, the magnitude of δ should not be considered so much as the fact that $\delta \sim \ell^{\frac{1}{2}}$ for zero incidence, while $\delta \sim \ell^{3/4}$ for the flat plate at 15° (both bluntnesses). This comparison is consistent with the fact that the mass flow in the present boundary layer is only a fraction of Kendall's value[20] (Figs. 18b and 19b).

The measured 3/4 power growth over the plate at an angle of attack is characteristic of strong viscous-inviscid interaction as compared to $\frac{1}{2}$ power growth in the weak interaction regime. Little can be concluded, however, because of the "irregular" pressure distribution over this configuration. In fact, in view of the relatively weak negative pressure gradient previously mentioned for this region ($p \sim \ell^{-\frac{1}{4}}$), one possible explanation for the fast boundary layer growth might be the commonly known thickening which precedes separation from the surface. It therefore appears that the boundary layer thickness, as well as the pressure distribution, is affected by the separation interaction some distance upstream of the separation point.

IV. 3. Separated Flow Region

The initial experiments used the thin oil film technique of flow visualization to determine if and where the boundary layer separated on the leeward side of the model with the sharp leading edge as the angle of attack to the freestream was increased. The results are shown in Fig. 23 along with those obtained for the leeward side of a wedge by the same technique.[16] On the flat plate, the point of separation moves from the trailing edge to less than half-chord at $\alpha = 22.5^{\circ}$ and $Re_{\infty L} = 133,000$. When the Reynolds number based on plate length and freestream conditions is decreased to $\simeq 78,000$, the separation point seems to occur further from the leading edge than in case of the larger Reynolds number.

As incidence is increased, it is expected that the point of boundary layer separation should move toward the leading edge since the windward-leeward pressure ratio increases with increasing angle at attack. Wu[16] found comparable separation zones on the wedge when the leeward surface was inclined the same angle from the freestream direction (Fig. 22). However, for large angles of attack ($\alpha_{\text{leeward side}} > 15^{\circ}$), Wu's separation point moved closer to the leading edge than the separation point on the flat plate. An explanation may rest in the fact that the windward side of the 20°-wedge is compressing the freestream flow 20° more than the leeward side expansion and hence, at large angles of attack, the static pressure behavior in the near wake differs considerably from that of the flat plate.

Static Pressure

The separation region, in which the surface pressure rises from a minimum to somewhat of a plateau level at the trailing edge, is the first step in a two step recovery of pressure to the freestream value. The pressure rise process in the separation interaction is similar in form to the well known pressure distribution on a flat plate-ramp compression corner which has been studied by several authors including Chapman,[24] Lewis,[25] and Holden.[26] Chapman has correlated the pressure rise versus distance for different disturbances in supersonic flow in a so-called free interaction region in which the interaction is free from direct influences of downstream geometry. To show that the separated flow on the flat plate at an incidence is no exception to this rule, the present pressure data has been correlated together with measurements obtained by Lewis[25] on a ten-degree ramp. The nondimensional Chapman-parameters are

$$P = \frac{C_{p_0}(M_0^2-1)^{\frac{1}{4}}}{\sqrt{C_{f_0}}}$$

and

$$X = \frac{\ell-\ell_0}{\delta_0^*}\sqrt{C_{f_0}}\,(M_0^2-1)^{\frac{1}{4}} \quad .$$

They are based on conditions just ahead of the separation interaction region for both Lewis' and the present configuration. The comparison which is presented in Fig. 24 is quite satisfactory, at least in the initial region of pressure rise. However, the pressure does not rise to the same high plateau level as in the case of a long ramp. Hence,

it appears that the downstream conditions affect the latter part of the pressure rise after separation.

Comparison of the "plateau pressure" with wall-pressure on leeward side of wedge

With regard to leeward side plateau-pressure, a comparison can be made with Wu's results for a wedge at an angle of attack.[16] For the 10-degree half angle wedge at a 25 degree incidence (meaning the leeward side was inclined 15^{o} from the freestream flow), Wu measured a base pressure $\frac{p_b}{p_\infty} = .43$ for comparable $Re_{\infty L}$ and M_∞ as in the present experiment. This is almost identical with the pressure measured at the trailing edge of the thin flat plate. Also, for the above wedge conditions, the observed separation point $(\frac{\ell_{sp}}{L})_{wedge} = .64$ while for the sharp flat plate with the same leeward incidence, $(\frac{\ell_{sp}}{L}) = .68$. Pressure orifices on the leeward wedge surface showed that the pressure in the separation zone was nearly identical with the base pressure. The wedge leading edge thickness was estimated to be no more than .002 in.

These comparisons suggest that for comparable freestream conditions, the flow conditions on the leeward side of a thin flat plate and wedge are similar, for any moderate wedge angle, when the two surfaces are inclined the same angle from the freestream direction. The flows on the windward sides, which are quite different in the two cases only act to separate the flow on the leeward side but do not affect it otherwise.

Effect of Leading Edge Bluntness

It is evident from Fig. 16 that the influence of the leading edge is not confined to the first region, but also effects the second region where the flow separates from the surface. The location of minimum pressure shifted from $\ell/L \simeq .5$ for the sharp model to $\ell/L \simeq .6$ for the blunter model. Also, it was observed with the flow visualization that separation moved from $(\ell_{sp}/L) \simeq .67$ for t = .0005 in. to $(\ell_{sp}/L) \simeq .75$ for the thicker leading edge. This behavior can be explained, at least in part, by the fact that the blunter leading edge creates a larger favorable pressure gradient to "compete" with the adverse gradient created by the forward pressure diffusion from the trailing edge.

In a recent publication of his experiments, Holden[26] has demonstrated the role of Cheng's bluntness-viscous interaction parameter,[11] $\chi_\epsilon/(\kappa_\epsilon)^{\frac{2}{3}}$, in the behavior of separation on a flat-plate ramp configuration.

In the present experiment, $\chi_\epsilon/\kappa_\epsilon^{\frac{2}{3}} = 1.35$ for t = .0005 in., and $\chi_\epsilon/\kappa_\epsilon^{\frac{2}{3}} = 0.34$ for t = .004 based on $M_\infty = 6.14$, $Re_\infty/in. = 186,000$, and a characteristic length of ℓ = .05 in. (half chord); where

$$\chi_\epsilon = \epsilon(0.664 + 1.73\, T_w/T_{t\infty})M_\infty^3\,(C/Re_\ell)^{\frac{1}{2}}$$

$$\epsilon = \frac{\gamma-1}{\gamma+1}, \quad \gamma = 1.4$$

and

$$\kappa_\epsilon = \epsilon\,\kappa\,M_\infty^3\,t/\ell$$

$$\kappa = D_N/\tfrac{1}{2}\rho_\infty\,u_\infty^2\,t$$

The nose drag was based on the pressure distribution measured on a flat leading edge at a 15^{o} incidence and Mach 6 flow by Goldberg et al.[27] Note that if the tip of the sharp model is cylindrical instead of flat, the drag is decreased by about a factor of 2, and $(\chi_\epsilon / \kappa_\epsilon^{\frac{2}{3}})$ becomes approximately 2.15.

Holden found that for the ramp with $(\chi_\epsilon / \kappa_\epsilon^{\frac{2}{3}}) < 0.5$, increase in bluntness caused a marked decrease in the length of the separated region. This same result was found for the thin flat plate model (Fig. 23), i.e. the separation point moved toward the trailing edge for the t = .004 in. tip. Not enough data were obtained to correlate with Holden's result that the separation point moved toward the leading edge with increased bluntness if $\chi_\epsilon / \kappa_\epsilon^{\frac{2}{3}} > 0.5$.

In view of the results from the present experiment, the blunt tip plays the following role in affecting the boundary layer separation: The strong bow shock through which the streamlines at the boundary layer edge have passed reduces the edge Mach number, so that separation would occur sooner since there is less momentum.

However, on the leeward side of the inclined plate, the boundary layer edge unit Reynolds number is decreased which has the effect of postponing separation.[25] More importantly, however, the tip bluntness introduces a more favorable pressure gradient (Fig. 16) which helps to resist the adverse pressure gradient produced by the diffusion of pressure forward from the trailing edge. These latter effects are therefore assumed predominant in decreasing the separation region as the leading edge thickness is increased from .0005 in. to .004 in.

Velocity and Total Temperature in Separation Region

After the boundary layer separates from the leeward surface, the flowfield within the separation region is very difficult to define experimentally since there can be no certainty about data obtained with a unidirectional probe such as the Pitot pressure probe. The values of y at which the velocity goes to zero (Fig. 25) are the first points at which the Pitot pressure is equal to the static pressure measured at that station.

One measurement which was not sensitive to flow direction, as long as the flow remained two-dimensional, was the recovery temperature of the hot wire. Assuming that the temperature of the plate surface in the recirculating flow remains uniformly equal to the recovery temperature of the surface upstream of the separation, then the normalized total temperature profiles are as shown in Fig. 26. The distance above the surface for which the total temperature remains close to the recovery temperature grows with increasing ℓ/L. This indicates that the vertical dimension of the recirculation flowfield grows until some point downstream of the trailing edge.

Two final considerations should be given to the separated flow region. First, it is possible that the flow is not completely steady and that there may be some "pulsing" of the separation shock and bubble flow. Chang[2] refers to several authors which have examined this phenomenon. Since all of the measurements in this experiment recorded only mean quantities, any unsteadiness is not detected.

A second possibility, which is manifestly important in wake flow, is the transition from laminar to turbulent flow in the separation

and reattachment process. It was presupposed in this discussion that the flow over the leeward surface remained laminar, and Appendix B cites evidence to show that, in fact, the flow remains laminar at least as far back as the data station furthest downstream in the wake.

IV. 4. Laminar Wake Flow Region

The data reduction technique described in Section III. 4. for the viscous boundary layer region prior to separation was also used to reduce the measurements in the inner, or viscous, wake flow.

Velocity profiles at stations x/L = .1, .2, and .35 are shown in Fig. 25; and stations x/L = .5, 1.0, 1.5, and 2.0 are presented in Fig. 27. It can be seen in Fig. 25 that the rear stagnation point is located between x/L = .1 and .2. The wake velocity profiles, along with the temperature excess and Mach number distributions in Figs. 28 and 29, are presented for ranges of y where it can be assumed that the static pressure does not vary significantly from the pressure measured at point of minimum velocity (Fig. 14).

A striking feature here is that although a significant velocity defect remains in the viscous wake for several plate lengths (Fig. 27), the velocity profiles for x/L > .5 seem to have lost most of their asymmetric properties. Small differences, however, can be seen between the two wake edge values.

The differences between the viscous wake edge properties is illustrated best by the Mach number profiles in Fig. 29. The Mach number on the windward side is typically ten percent lower than on the leeward side. This fact indicates a greater total pressure loss for streamlines passing on the windward side of the model than on the

leeward side. This result shows another inadequacy of the inviscid shock-expansion model, in Fig. 1, which predicted that the wake edge Mach number on the windward side is larger than on the leeward side. This contrast with the experimental case shows that there is less total pressure loss on the experimental leeward surface through the two-shock system (separation plus wake shock, see Fig. 12) while streamlines on the windward side also experience a wake shock not accounted for in the inviscid model.

Upwash in Near Wake

Another interesting observation is that the line of minimum velocity in the wake for $x/L \geq .5$ has a positive slope to the freestream direction. Wu[16] found a similar result behind a wedge plus the fact that the dividing streamline (i. e., the streamline which divides the windward and leeward side flow) had an even greater positive slope than the minimum velocity line. If the same holds true in the present flow, then there is an upwash in the near wake as already found from the simple inviscid flow model in the introduction (Fig. 1).

Comparison of Wake Properties with Those of a Wedge at Angle of Attack and a Symmetric Flat Plate

Figures 30 and 31 show the minimum velocity and maximum temperature along the wake compared to the wake of a similar flat plate at zero angle of attack.[15] Also compared in these figures are the wake centerline properties behind a 20° wedge whose leeward surface is inclined 15° from the freestream direction. It was concluded in Section IV. 3. that the flow on the leeward surfaces of the wedge and flat plate are quite similar. However, it is quite evident that the wake

properties of these two configurations differ considerably, which is due to the greater flow compression on the windward side of the wedge.

Batt and Kubota[15] made a comparison between the flat plate and slender wedge at zero angle of attack, and they found that the velocity defect behind the wedge was greater at the beginning of the wake, but the centerline velocity increased faster with distance than for the flat plate. The same qualitative comparison can be deduced from Fig. 30 for the flat plate and wedge at the same angle of attack.

As shown also in Fig. 30, the minimum velocity in the wake of the flat plate at angle of attack is nearly the same as the minimum velocity behind Batt and Kubota's thin flat plate aligned with the freestream. This comparison must be qualified, however, with the fact that Batt and Kubota measured a wake center total temperature at $x/L = 1$ to be about 10 percent lower than the freestream total temperature in this region. In the present results, it was assumed that $T_t = T_{t\infty}$ throughout the entire wake. If one assumes that $T_t = .9\ T_{t\infty}$ at $x/L = 1$ in the wake center behind the inclined flat plate as well, then the minimum velocity values are decreased by about 5 percent while the maximum static temperature curve is adjusted upward by about 10 percent. After making this adjustment of the wake centerline values behind the plate at an angle of attack, the wake velocity and temperature still show the same growth or decay rate as the wake velocity at zero angle of attack, but the velocity is smaller and the temperature larger than in the wake without angle of attack.

V. SUMMARY OF RESULTS

Experimental measurements of the mean flow quantities over the leeward surface and in the near wake of a one inch adiabatic thin flat plate at a 15^{o} angle of attack were obtained at Mach 6 and a free-stream Reynolds number Re_{L} = 186, 000 based on the chord length. The leading edge thickness of the flat plate model was t = .0005 in. and .004 in. The measurements included Pitot pressure and static pressure distributions and mean hot-wire measurements. The main results of this investigation are as follows.

Surface Static Pressure Measurements

The size and thickness of the plate was too small for surface pressure taps, therefore a cone-cylinder probe bent to the proper angle of attack was used to measure the static pressure on the plate surface. Various calibrations showed this technique to be sufficiently accurate.

Leeward Side Flow Field and Pressure Distribution

The viscous-inviscid flow interaction on the leeward surface gives a pressure distribution which is entirely different from the inviscid Prandtl-Meyer expansion. Three distinct regions are identified: the leading edge interaction region, where the pressure decays and is very sensitive to the leading edge bluntness; the separation region in which the pressure rises to a first "plateau"; and the near wake region in which the pressure rises again to a second plateau which is nearly equal to the freestream pressure.

Leading Edge Interaction Region

Simple flow models show that in the leading edge interaction

region, not only viscous inviscid flow interaction and leading edge bluntness are important but also that the separation interaction is felt considerably further upstream than where the boundary layer actually separates from the surface. The growth of almost the entire attached laminar boundary layer is $\delta \sim \ell^{3/4}$ for $.1 \leq \frac{\ell}{L} \leq .5$ for both bluntnesses and the pressure decay is $\frac{p}{p_\infty} \sim \ell^{-\frac{1}{4}}$ for $.25 \leq \frac{\ell}{L} \leq .5$.

Streamlines which pass through the bow shock near the leading tip enter the boundary layer far downstream and detailed data analysis of two stations upstream of separation show that flow quantities in the entropy layer change significantly with a very small increase in the leading edge bluntness. Despite the sharp pressure and temperature gradients in the entropy layer, there still remains a distinct boundary layer where viscosity and heat transfer effects are important in contrast to a rotational inviscid flow in the entropy layer. It is shown that vorticity interaction is unimportant.

Separation Location

The separation point was found as plate incidence was varied from 0^o to 22.5^o. The results were compared to a wedge whose leeward surface was inclined the same angle from the freestream, and they showed that (1) the details of the flow on the windward side play a minor role in determining separation and thus the pressure distribution on the leeward side, and (2) decreasing the Reynolds number increases the resistance to separation, a result found also for hypersonic boundary layers over a flat plate followed by a ramp.

Free Interaction Pressure Correlation

The two stage pressure recovery to the freestream value is

similar to the pressure rise in laminar flow which has separated from and reattached to the flat plate-ramp model. Using a correlation due to Chapman, the present results in the "free interaction" region compare favorably to the results obtained by Lewis with a flat plate-ramp configuration.

Flow Profiles in Separation and Near Wake Region

Although quantitative results within the small recirculating flow are not possible, the surrounding flowfield and approximate dimensions of the separated region were determined. For $\alpha = 15^{o}$, the rear stagnation point occurs around $\frac{x}{L}_{R.ST.} = .15$. The following wake centerline is located above the trailing edge and has a positive slope with respect to the freestream, indicating an upwash in the near wake. The wake centerline properties of the flat plate at $\alpha = 15^{o}$ grow similarly to those behind a flat plate at zero angle of attack, but contrasts with the higher streamwise gradients behind the wedge at angle of attack.

REFERENCES

1. Korkegi, R. H.: "Viscous Interactions and Flight at High Mach Numbers," ARL 70-0124, (July, 1970).

2. Chang, P. K.: Separation of Flow, Pergamon Press, 1970.

3. Kaufman, L. G., Hartoflis, S. A., Evans, W. J., Oman, R. A., Meckler, L. H., Weiss, D.: "A Review of Hypersonic Flow Separation and Control Characteristics," ASD-TDR-62-168 (March, 1962).

4. Bertram, M. H., Fetterman, D. E., Henderson, A., Johnston, P. J.: "Studies Relating to the Attainment of High Lift-Drag Ratios at Hypersonic Speeds," NASA TN D-2956 (August, 1965).

5. Bertram, M. H.: "Hypersonic Laminar Viscous Interaction Effects on the Aerodynamics of Two-Dimensional Wedge and Triangular Planform Wings," NASA Tn-D-3523 (August, 1966).

6. Ferrari, C.: "Airfoil Pressures at Supersonic Speeds Under Separated Flow Conditions," Applied Physics Lab., The Johns Hopkins University (August 1957).

7. Klineberg, J. M., Kubota, T., Lees, L.: "Theory of Exhaust-Plume/Boundary-Layer Interactions at Supersonic Speeds," AIAA Paper No. 70-230, AIAA 8th Aerospace Sciences Meeting, New York, New York, January 19-21, 1970.

8. Bertram, M. H., Baradell, D. L.: "The Blunt Plate in Hypersonic Flow," NASA TN D-408 (October, 1960).

9. Lee, J. D., Gregorek, G. M., Nark, T. C.: "An Experimental Investigation of the Surface Pressure and the Laminar Boundary Layer on a Blunt Flat Plate in Hypersonic Flow," ASD-TDR-62-792 (March, 1963)

References (Continued)

10. Bertram, M. H., Henderson, A.: "Effects of Boundary-Layer Displacement and Leading-Edge Bluntness on Pressure Distribution, Skin Friction, and Heat Transfer of Bodies at Hypersonic Speeds," NACA TN 4301 (July, 1958).

11. Cheng, H. K., Hall, J. G., Golian, T. C., Hertzberg, A.: "Boundary-Layer Displacement and Leading-Edge Bluntness Effects in High-Temperature Hypersonic Flow," Journal of the Aerospace Sciences, Vol. 28, No. 5, pp. 353-381 (May 1961).

12. Lee, J. D.: "Viscous Effects on Blunt Plates at Hypersonic Speeds," ARL 70-0006 (January 1970).

13. Stollery, J. L.: "Hypersonic Viscous Interaction - An Experimental Investigation of the Flow Over Flat Plate at Incidence and Around an Expansion Corner," ARL 70-0125 (July, 1970).

14. Allegre, J., Bisch, C.: "Angle of Attack and Leading Edge Effects on the Flow about a Flat Plate at Mach Number 18," AIAA Journal, Vol. 6, No. 5, pp. 848-852 (May, 1968).

15. Batt, R. G. and Kubota, T.: "Experimental Investigation of Laminar Near Wakes behind 20° Wedges at $M_\infty = 6$," AIAA Journal, Vol. 6, No. 11, pp. 2077-2083 (1968); also "Experimental Investigation of Far Wakes behind Two-Dimensional Slender Bodies at $M_\infty = 6$," AIAA Journal, Vol. 7, No. 11, pp. 2064-2071 (1969). Also Batt, R. G.: "Experimental Investigation of Wakes behind Two-Dimensional Slender Bodies at Mach Number Six," Ph. D. Thesis, California Institute of Technology, Pasadena, California (1967).

References (Continued)

16. Wu, J. J., and Behrens, W.: "An Experimental Study of Hypersonic Wakes Behind Wedges at Angle of Attack," AIAA Paper No. 71-563, AIAA 4th Fluid and Plasma Dynamics Conference, Palo Alto, California (June 21-23, 1971).
Also Wu, J. J.: "An Experimental Study of Wakes Behind Wedges at Angle of Attack," Ae. E. Thesis, California Institute of Technology, Pasadena, Calif. (1971).

17. Igawa, Hideo: Graduate Student, California Institute of Technology, Private Communication.

18. Behrens, W.: "Viscous Interaction Effects on a Static Pressure Probe at M = 6," AIAA Journal, Vol. 1, No. 12, pp. 2364-2366 (1963).

19. McCarthy, J. F., Jr. and Kubota, T.: "A Study of Wakes Behind a Cylinder at M = 5.7," AIAA Journal, Vol. 2, No. 4, pp. 626-629 (1964). Also McCarthy, J. F. Jr.: "Hypersonic Wakes," Ph.D. Thesis, 1962, California Institute of Technology, Pasadena, California.

20. Kendall, J.: "An Experimental Investigation of Leading-Edge Shock-Wave/Boundary-Layer Interaction at M = 5.8," Journal of the Aeronautical Sciences, Vol. 24, No. 1, p. 47 (Jan., 1957).

21. Ramaswamy, M. A.: "Experimental Investigation of the Effect of Cooling on Near Wake of Circular Cylinder at Mach Number Six," Ph.D. Thesis, California Institute of Technology, Pasadena, California (1971).

References (Continued)

22. Korkegi, R. H.: "Transition Studies and Skin Friction Measurements on an Insulated Flat Plate at a Hypersonic Mach Number," GALCIT Memo No. 17, California Institute of Technology, Pasadena, California (July, 1954).

23. Hayes, W. D. and Probstein, R. F.: Hypersonic Flow Theory, Academic Press, New York (1959).

24. Chapman, D. R., Kuehn, D. M. and Larson, H. K.: "Investigation of Separated Flows in Supersonic and Subsonic Streams with Emphasis on the Effect of Transition," NACA TN 3869 (March, 1957).

25. Lewis, J. E., Kubota, T., Lees, L.: "Experimental Investigation of Supersonic Laminar, Two-Dimensional Boundary Layer Separation in a Compression Corner With and Without Cooling," AIAA Journal, Vol. 6, No. 1 (January, 1968).
Also Lewis, J. E.: "Experimental Investigation of Supersonic Laminar, Two-Dimensional Boundary Layer Separation in a Compression Corner With and Without Cooling," Ph.D. Thesis, California Institute of Technology, Pasadena, California (1967).

26. Holden, M. S.: "Boundary-Layer Displacement and Leading-Edge Bluntness Effects on Attached and Separated Laminar Boundary Layers in a Compressible Corner. Part II: Experimental Study," AIAA Journal, Vol. 9, No. 1 (1971).

27. Goldberg, T. J., Ashby, G. C. Jr., Hondros, J. G.: "Center-Line Pressure Distributions on Two-Dimensional Bodies with Leading Edge Angles Greater Than for Shock Detachment at Mach No. 6 and Angles of Attack up to 25^{o}," NASA TN-D-1793.

28. Lees, L. and Probstein, R. F.: Hypersonic Flows of a Viscous Fluid (unpublished monograph with limited circulation), 1953, Brown University, Providence, R. I.

APPENDIX A

A MODEL FOR VISCOUS FLOW OVER LEEWARD SURFACE WITH BLUNT TIP

Inviscid Flow

This appendix outlines a simple, but instructive analysis which demonstrates the mechanism by which both the leading edge bluntness and viscous-inviscid interaction induce a large increase in pressure on the leeward surface of a flat plate at an angle of attack in hypersonic flow. For the present discussion, the effects of separation are not considered, but only the interaction region preceding boundary layer separation.

Lee[9] has considered a flat plate, with a cylindrical leading nose, at angles of attack. He used integral methods to analyze the viscous flow over the leeward surface for a distance of much less than 100 nose diameters downstream from the leading edge, and therefore his concern was also in a region strongly affected by the bow shock wave. Although the interaction of the strong curved shock wave with the boundary layer is important near the leading edge in the present experiment, it was shown in Part IV that this type of interaction was only of secondary importance over a majority of the preseparation surface, i.e. the vorticity in the entropy layer was small compared to the characteristic vorticity in the boundary layer. Lee did discover, however, that the form of the pressure on the leeward surface which was induced by the blunt tip followed the same functional dependence as that predicted by the similarity theory for blunt nosed slender bodies at zero angle of attack in inviscid hypersonic flow.[9]

For the present analysis, it was assumed that the edges of the flat plate model were cylindrical with diameters of t = .004 in. and .0005 in. (Section II. 2). Then the aforementioned pressure distribution on the leeward surface yields

$$\frac{p}{p_{t_2}} = \frac{\kappa}{(S/t)^{\frac{2}{3}}} + \frac{p_{\nu 15}}{p_{t_2}} \qquad \text{(A-1)}$$

where

p_{t_2} = total pressure behind a normal shock wave in the freestream flow.

$p_{\nu 15}$ = asymptotic pressure obtained through Prandtl-Meyer expansion from freestream

S = distance along the leeward surface from forward stagnation point

κ = empirical constant which is determined by knowing the pressure at the intersection of the nose and flat afterbody.

The pressure at the nose-afterbody junction was determined for the cylindrical nose followed by a plate at $\alpha = 15^{o}$ by picking the experimental value measured by Goldberg.[27]

Figure A-1 shows the inviscid flow pressure induced by the two different tips used in the present experiment based on Eq. A-1.

Viscous-Inviscid Flow Interaction

The next step is to calculate an additional contribution to the pressure which is induced by the growing boundary layer (viscous-inviscid flow interaction). First, it is assumed that the streamline which impinges on the forward stagnation point on the cylindrical nose (thereby passing through the normal part of the bow shock) is the same streamline which is adjacent to the leeward surface of the inviscid model.

Therefore, it is assumed that the total pressure at the edge of the leeward surface boundary layer is P_{t_2}, and the static pressure is also given by Eq. A-1 (Fig. A-1), so now the boundary layer edge Mach number and Reynolds number can be determined at any station along the surface. These quantities are denoted by the subscript "orig".

Based on the inviscid conditions just described, the boundary layer on the leeward surface is not in a region of strong interaction ($\bar{\chi}_{orig} < 3$), even at the station nearest to the leading edge. Following the method of Lees and Probstein[28] (see Hayes and Probstein,[23] p. 342), additional induced pressure p/p_{orig} is calculated according to weak viscous-inviscid interaction theory so that the final pressure for the present model is

$$\frac{p}{p_\infty}(\ell) = \frac{p}{p_{orig}(\ell)} \cdot \frac{p_{orig}(\ell)}{p_\infty}$$

$$= \frac{p_{orig}(\ell)}{p_\infty} \cdot (1 + .31\,\bar{\chi}_{orig} + .05\,\bar{\chi}^2_{orig}) .$$

This result is plotted for both bluntnesses in Fig. A-2.

In view of the simplifying approximations made in the analysis, the comparison with the measured pressures in Fig. 16 is not bad. The most crucial approximation is that the nose is cylindrical in shape. In this regard, the good comparison, especially for the blunt model, may be fortuitous and therefore misleading. But despite the fact that this analysis was idealized by many assumptions and that it was nothing more than a "superposition" of two separate effects, it does illustrate the mechanism which produces a large increase in leeward surface pressure over that which would exist with no bluntness and/or viscosity.

APPENDIX B

TRANSITION FROM LAMINAR TO TURBULENT FLOW

The Reynolds number, based on distance from the leading edge, of flow over the leeward surface of the flat plate model was small enough so that the flow remained laminar at least until boundary layer separation. If the viscous wake is initially laminar, then the velocity profiles render an unstable flow which somewhere downstream breaks down and becomes turbulent. In the absence of hot-wire fluctuation measurements, a quite reliable method of determining the point of transition in a hypersonic wake is to seek a rapid change in the rate of growth of the viscous wake width or a "sudden" drop of the wake center temperature due to turbulent mixing. No such transition point was detected for the configurations in this experiment (Figs. 12, 13, and 31) hence the conclusion can be drawn that either the wake remains laminar throughout the entire field measured, or that transition occurs before the viscous wake even forms.

To decide which of the two possibilities is the correct answer, Wu's transition results in the wake of the wedge at an angle of attack can be consulted.[16] Wu found that in general transition occurred several chord lengths downstream from the wedge base and that the transition point moved forward with greater leeward side velocity gradients which result when the vehicle angle of attack is increased. In particular, for the 20 degree wedge model mentioned in Fig. 23 at a 25^{o} incidence (its leeward side is then inclined 15^{o} from the free-stream direction), Wu found transition to be greater than one and one half chord lengths downstream from the wedge base by a small

extrapolation of the curve presented in Fig. 25 of his thesis. A comparison of the wake velocity profiles between this wedge configuration and the present flat plate model at a 15^{o} incidence shows that the velocity gradients behind the wedge are greater than those following the flat plate at the same downstream stations.

Therefore the conclusion for the flat plate wake in this experiment is drawn that transition from laminar to turbulent flow takes place at some distance in the wake beyond the stations at which data were obtained.

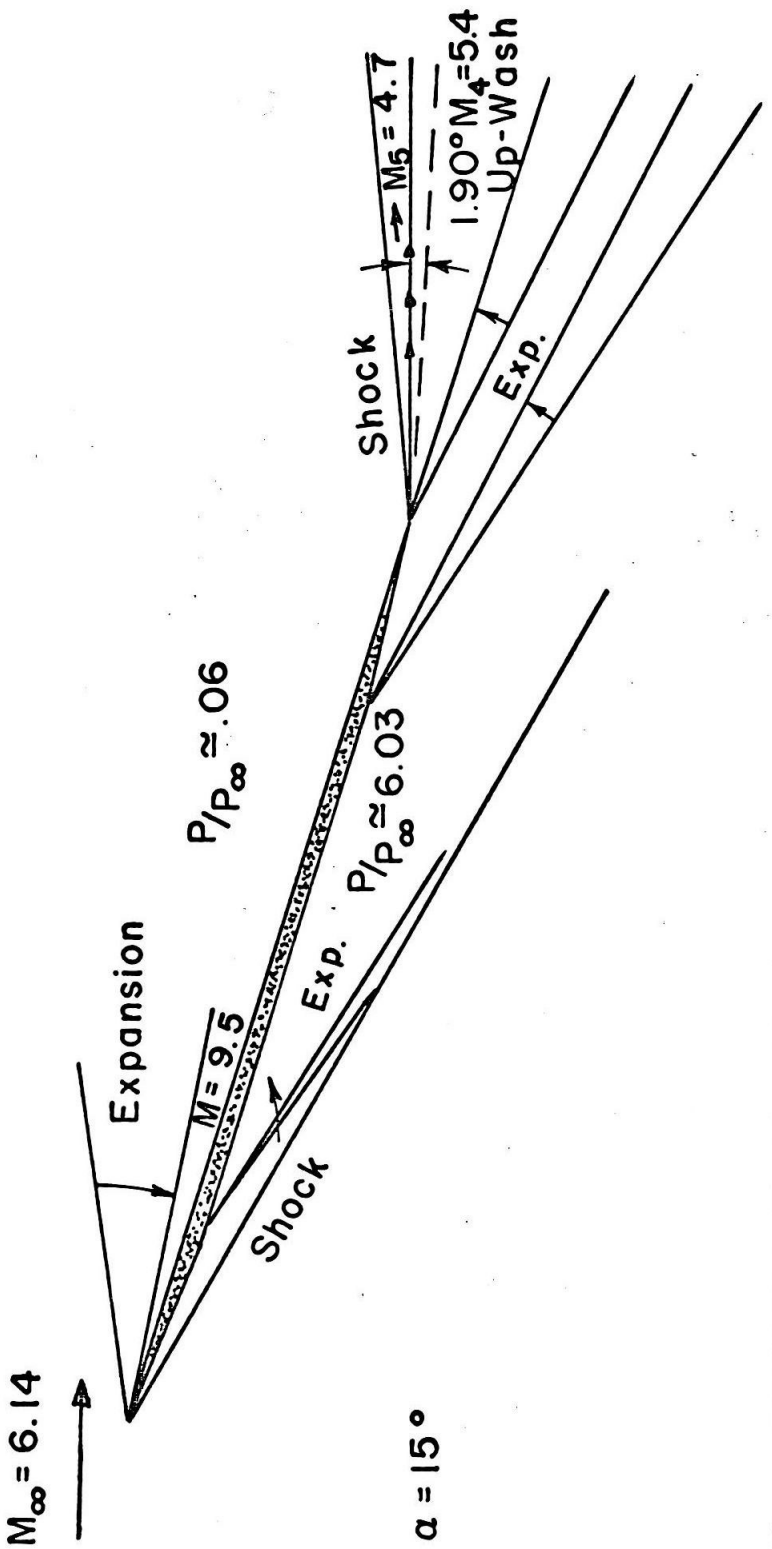

FIG. 1 INVISCID SHOCK-EXPANSION MODEL FOR BEVELED THIN FLAT PLATE AT AN ANGLE OF ATTACK

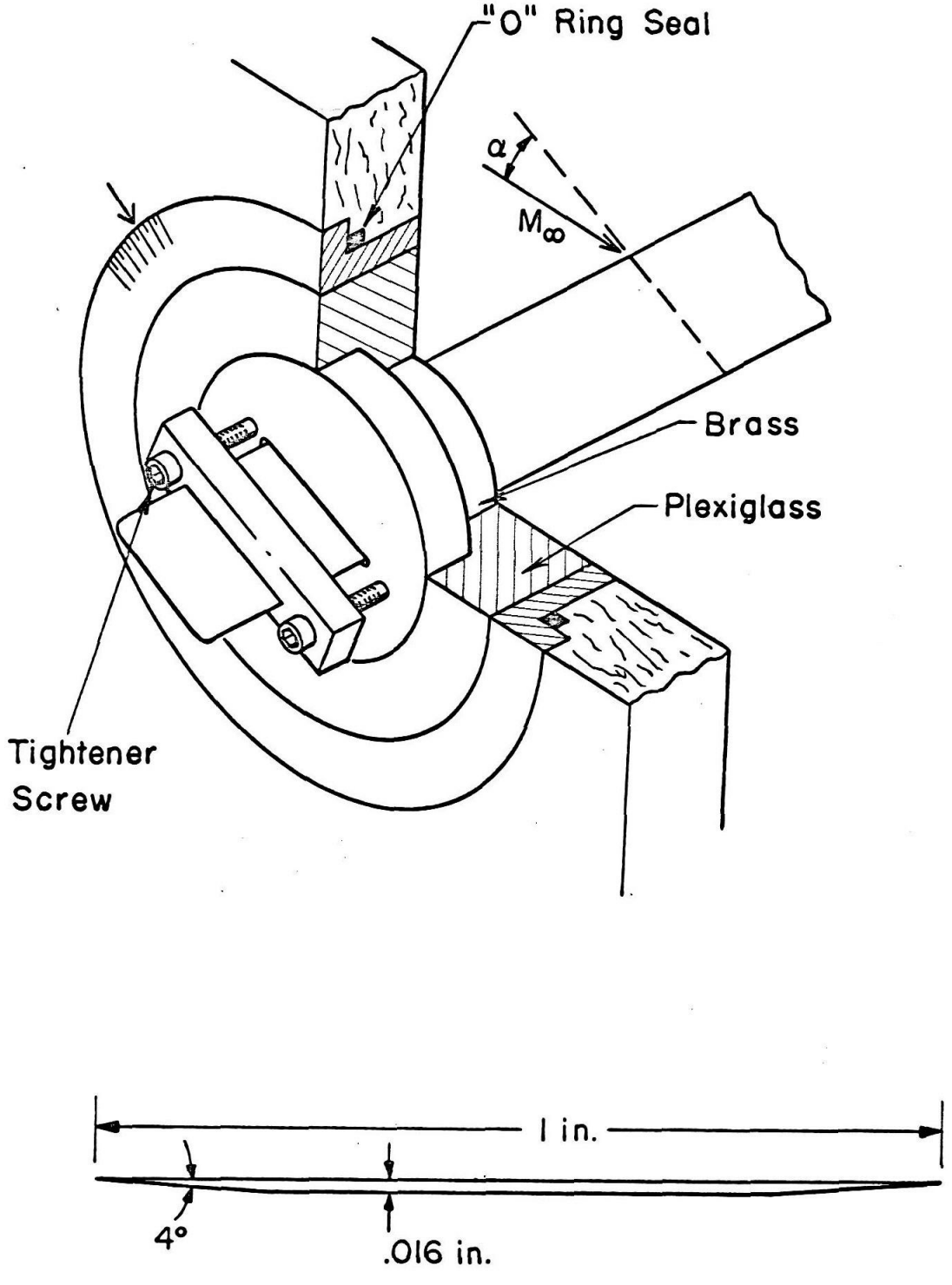

FIG. 2 MODEL CLAMP DEVICE AND DESIGN

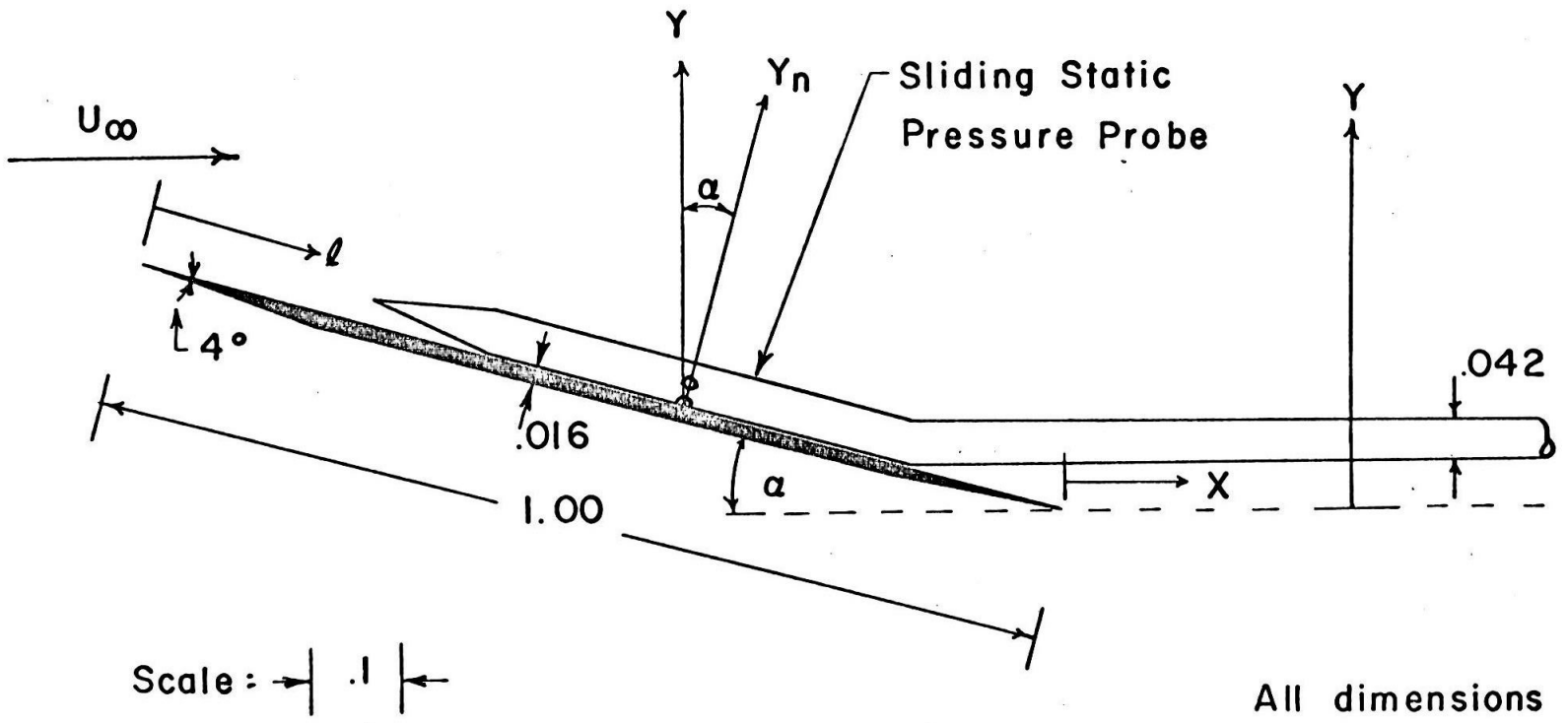

FIG. 3 FLAT PLATE AT INCIDENCE WITH STATIC PRESSURE PROBE

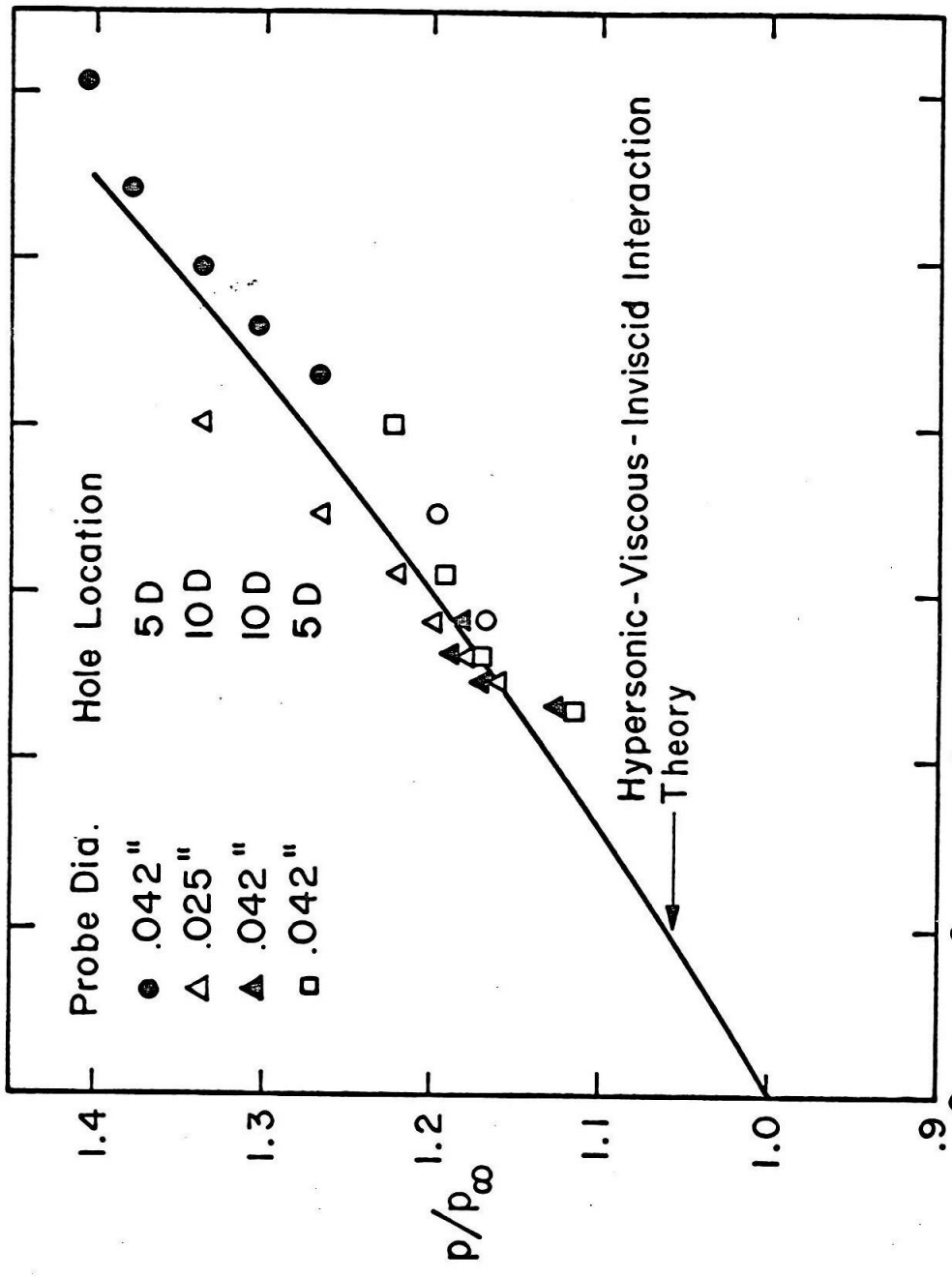

FIG. 4 COMPARISON OF SLIDING-STATIC PRESSURE PROBE MEASUREMENTS WITH HYPERSONIC VISCOUS-INVISCID INTERACTION THEORY

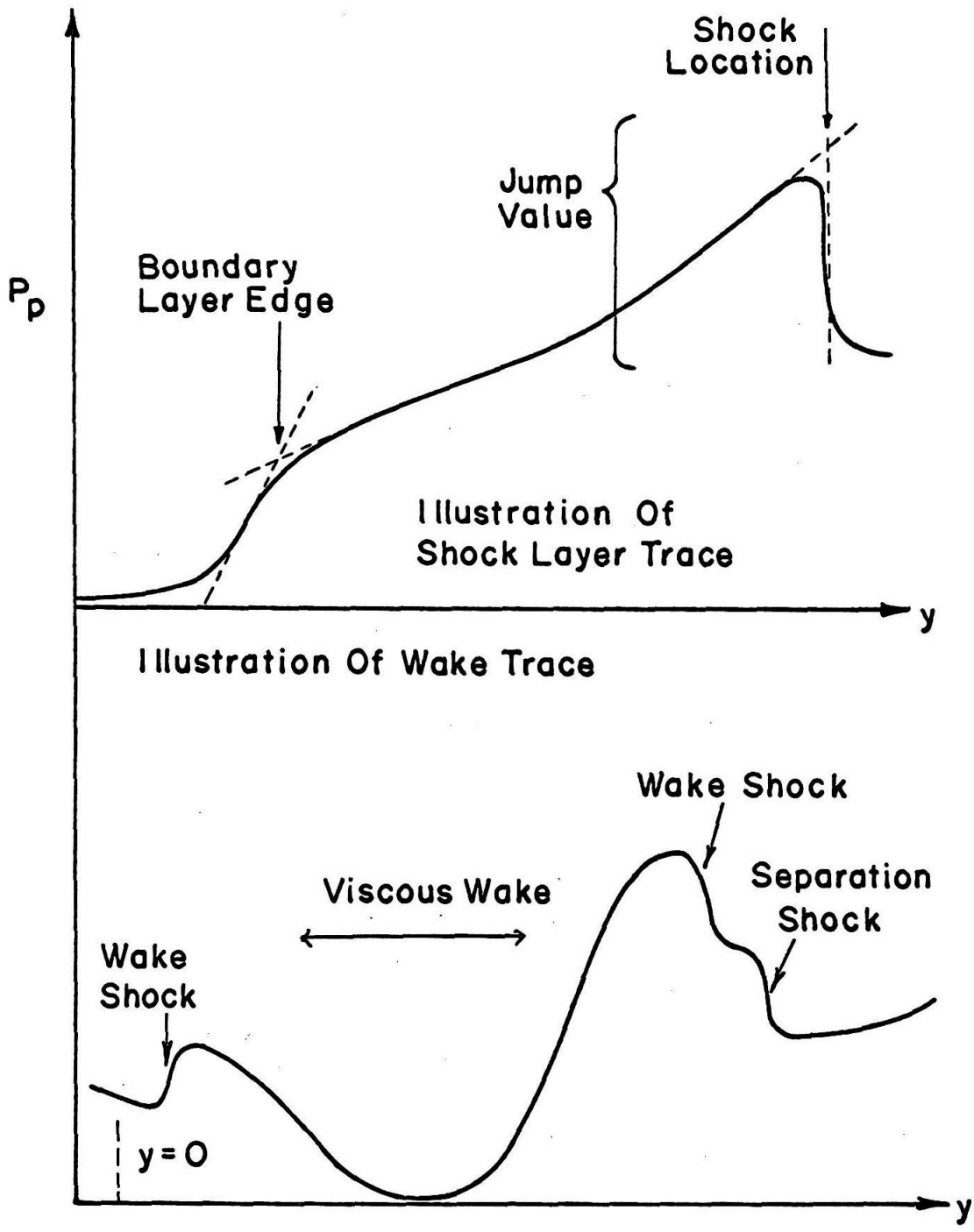

FIG. 5 ILLUSTRATION OF SHOCK LAYER AND WAKE PITOT PRESSURE TRACE

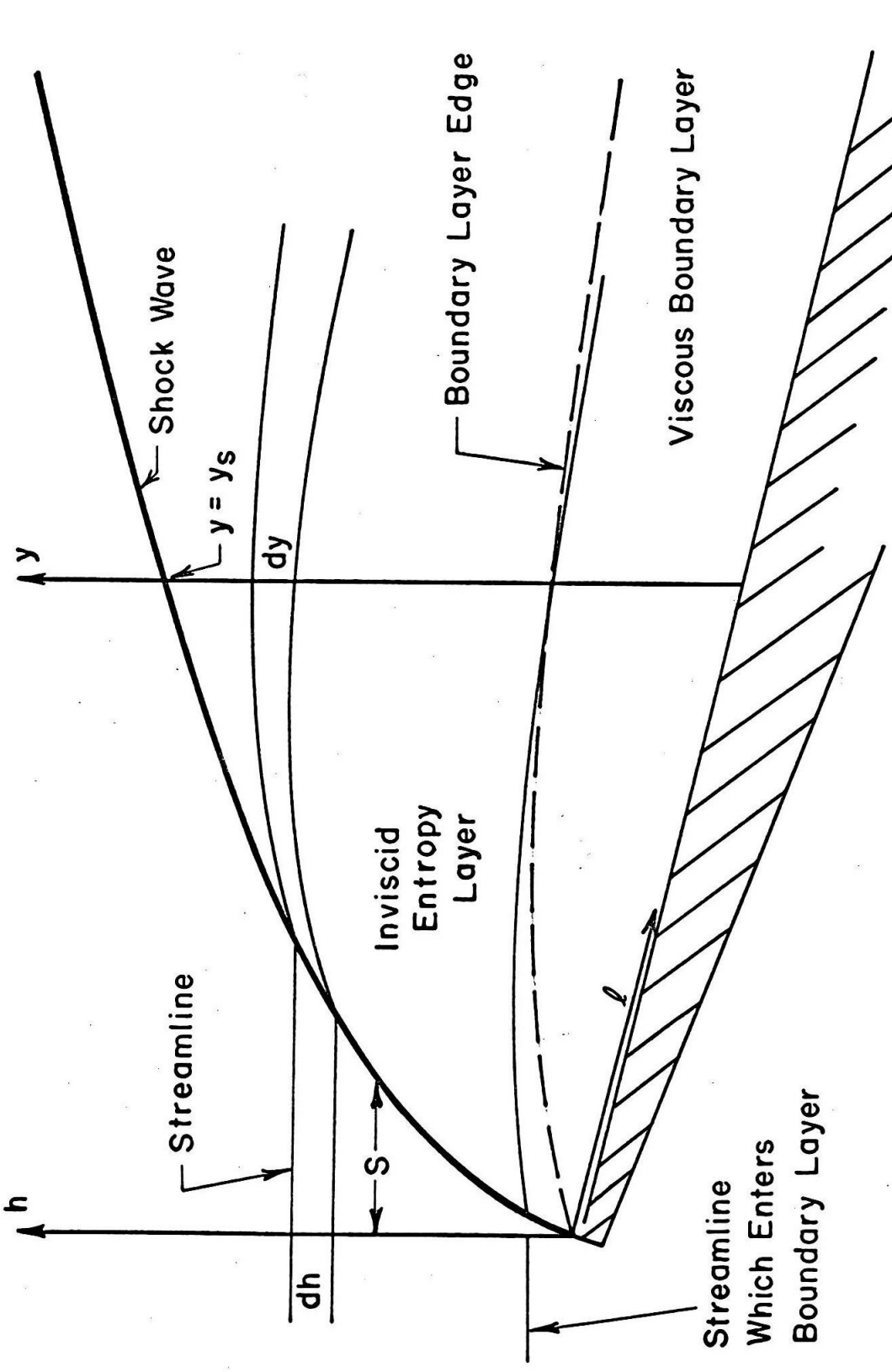

FIG. 6 NOMENCLATURE FOR DATA REDUCTION IN PRE-SEPARATION INTERACTION REGION

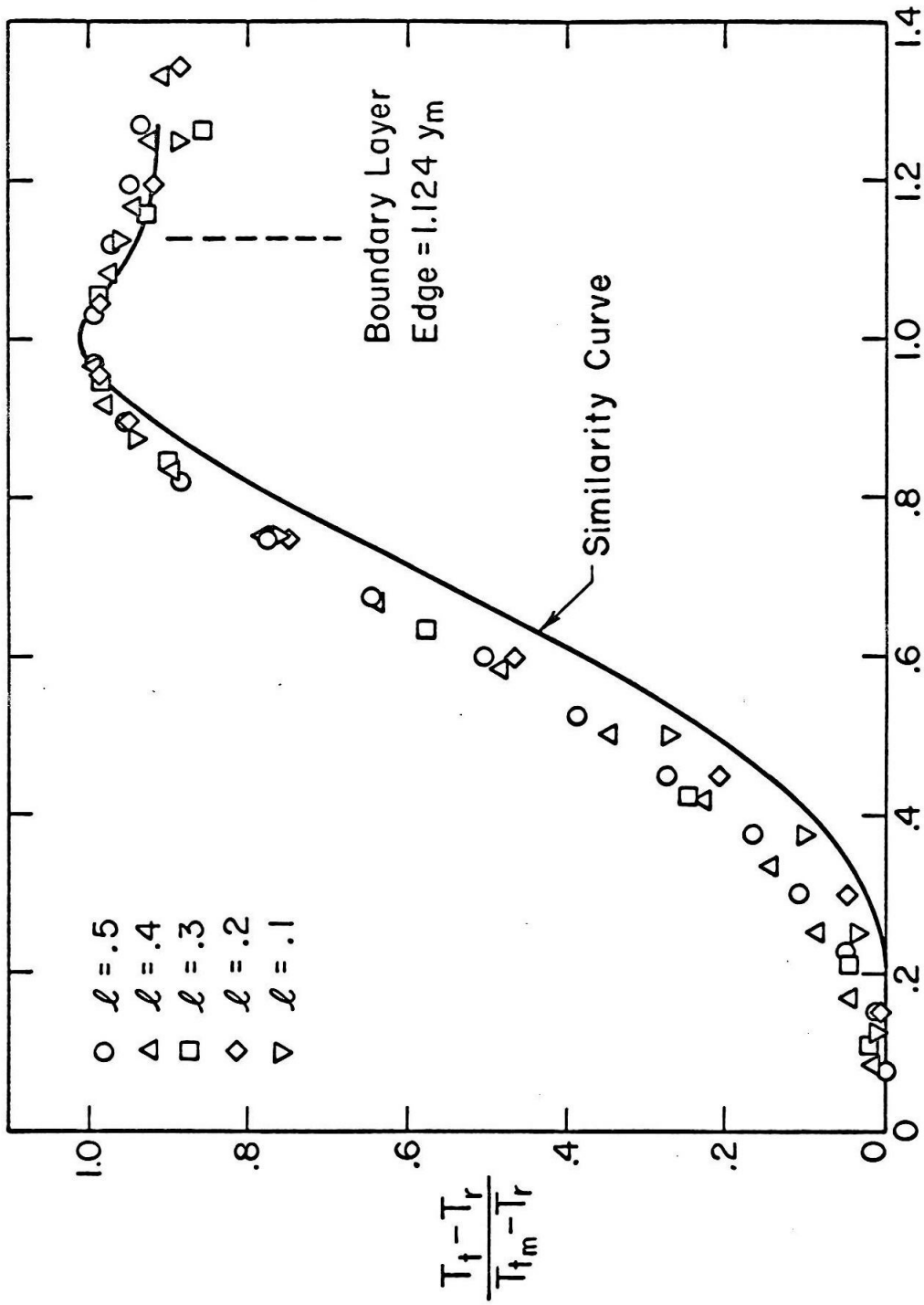

FIG. 7 NORMALIZED TOTAL TEMPERATURE DISTRIBUTION IN BOUNDARY LAYER PRIOR TO SEPARATION

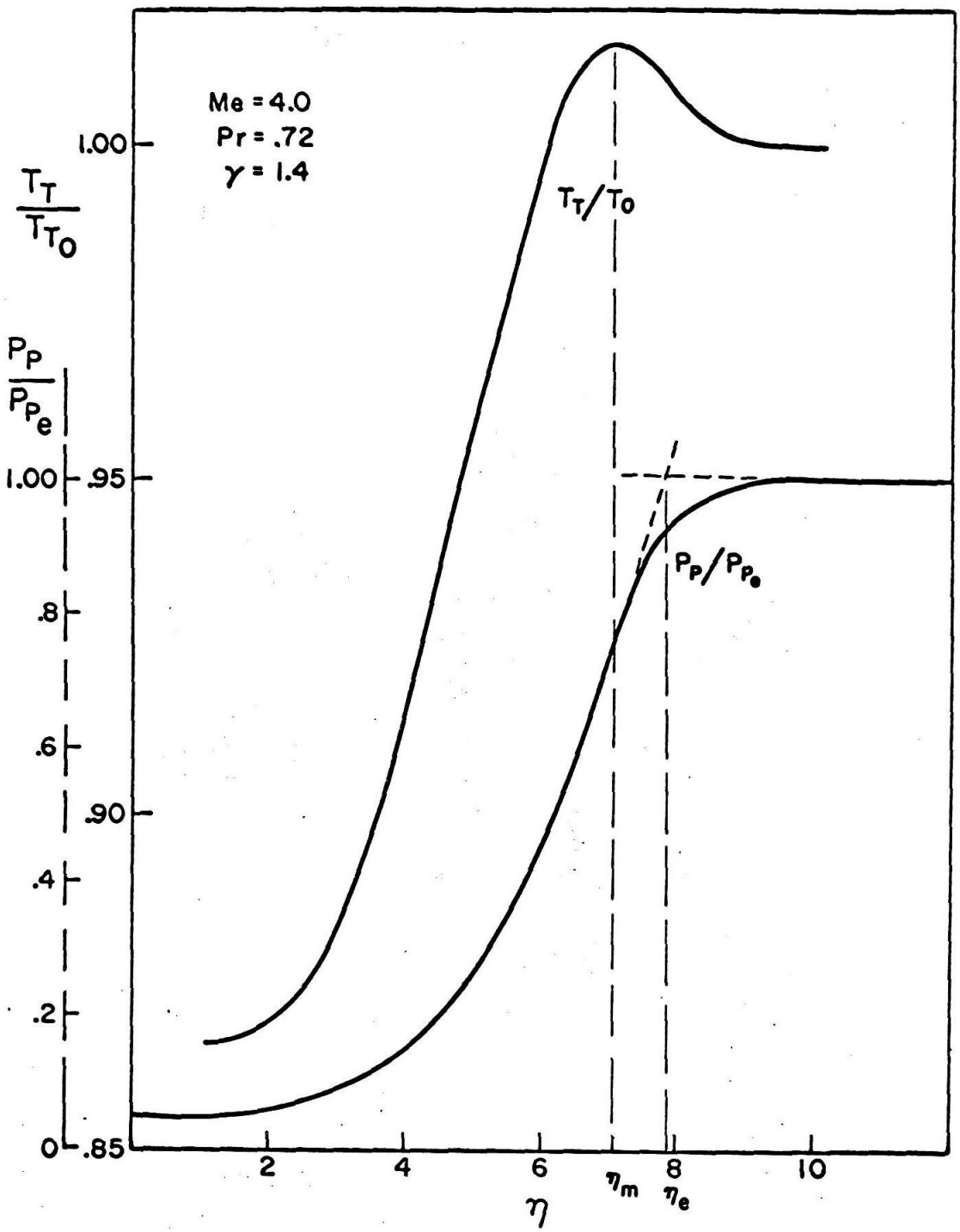

Fig. 8 Local Similar Solution for Compressible Blasius Boundary Layer

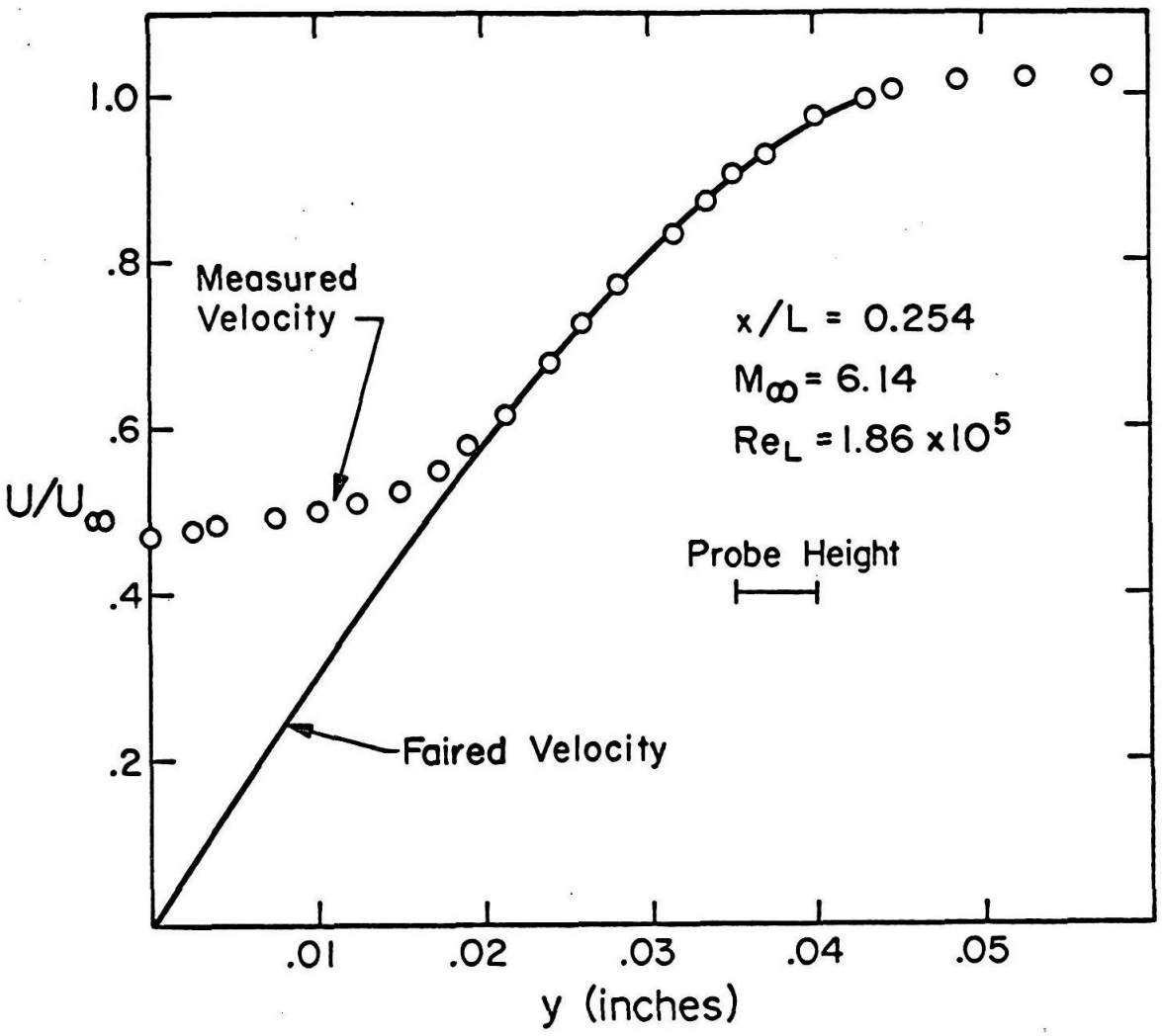

FIG. 9 MEASURED AND FAIRED VELOCITY PROFILE WITHIN ATTACHED BOUNDARY LAYER

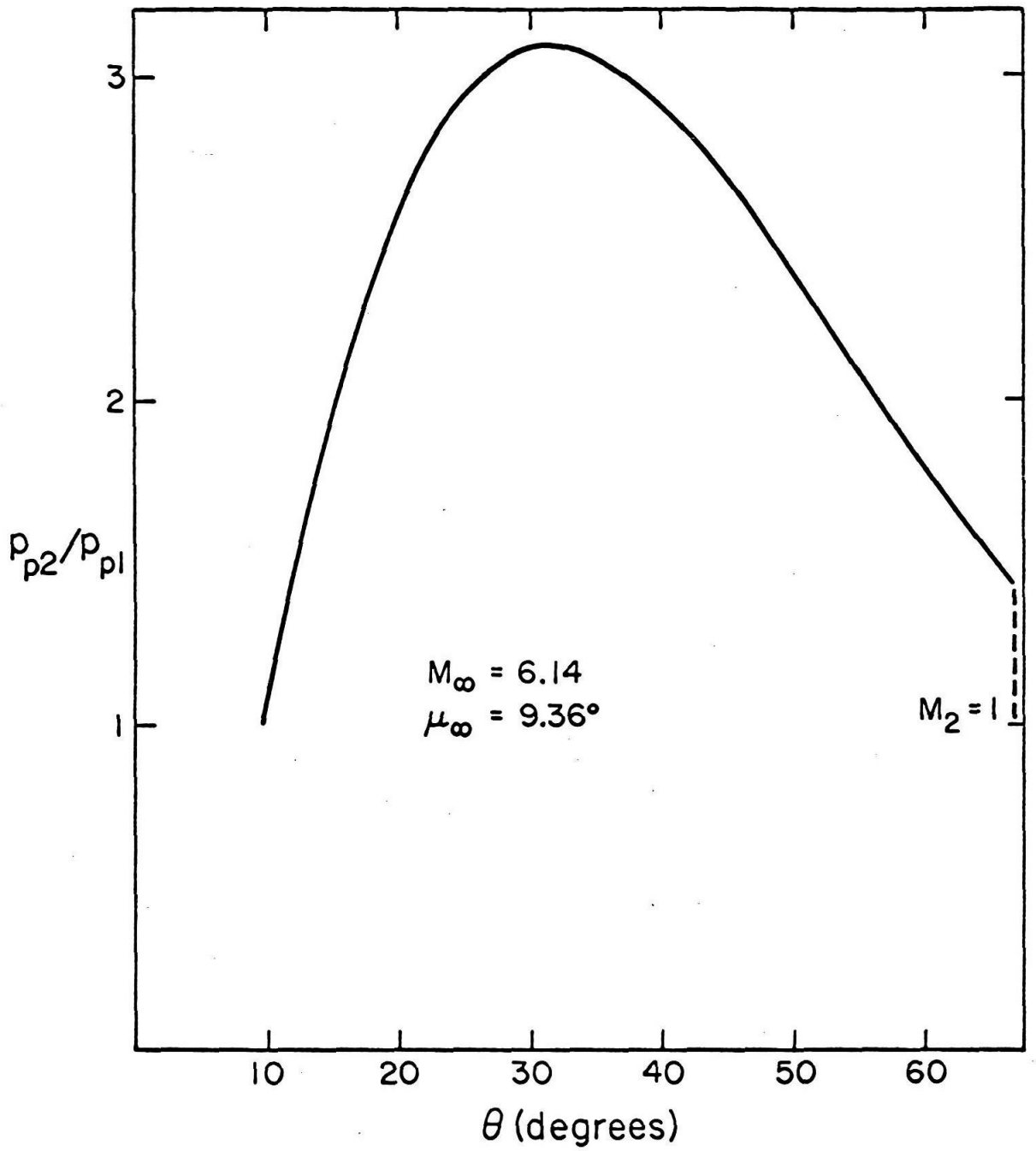

FIG. 10 PITOT PRESSURE RATIO ACROSS INCLINED SHOCKWAVE

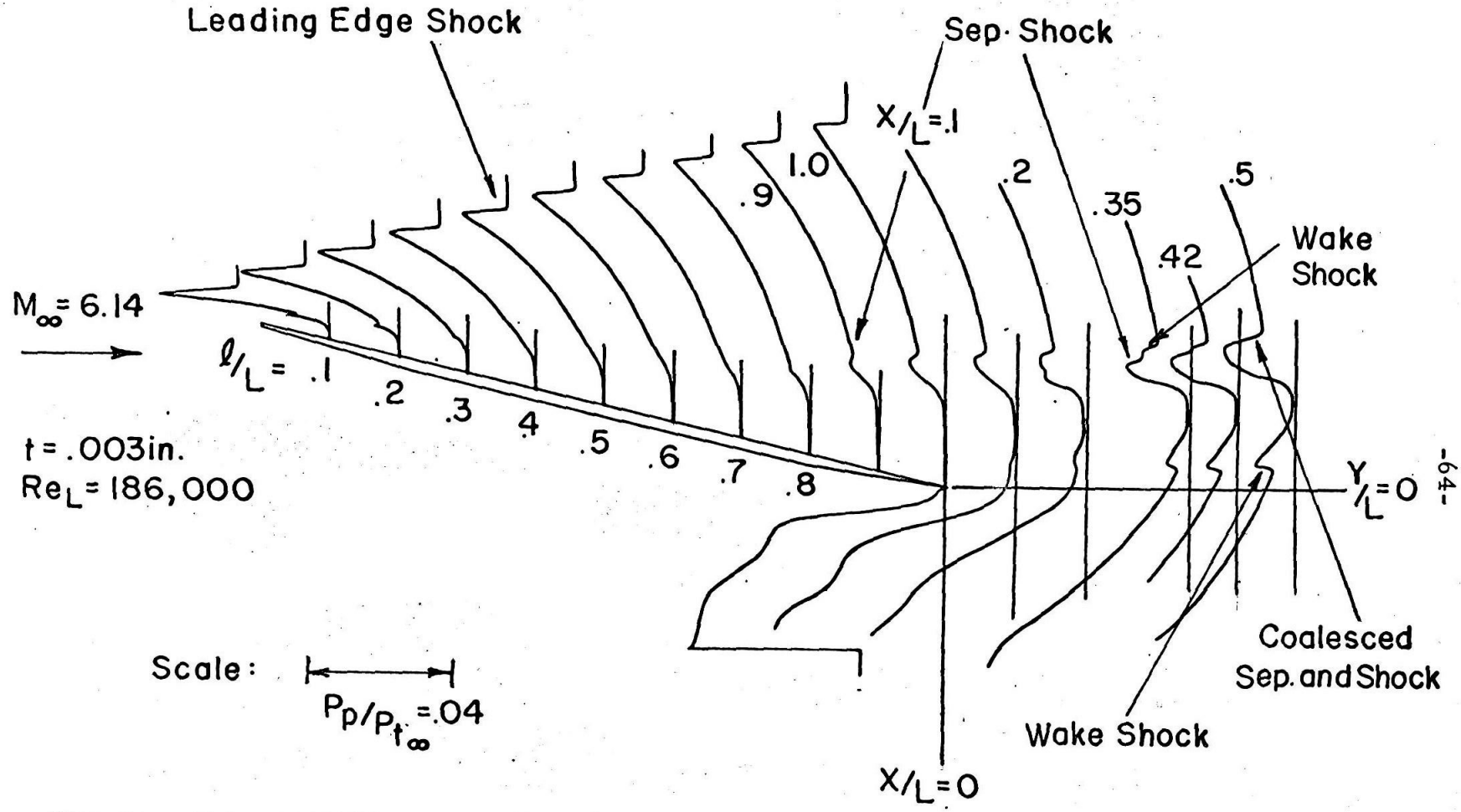

FIG. 11a EXPERIMENTAL PITOT PRESSURE TRACES OVER THE LEEWARD SURFACE OF A FLAT PLATE AT AN ANGLE OF ATTACK

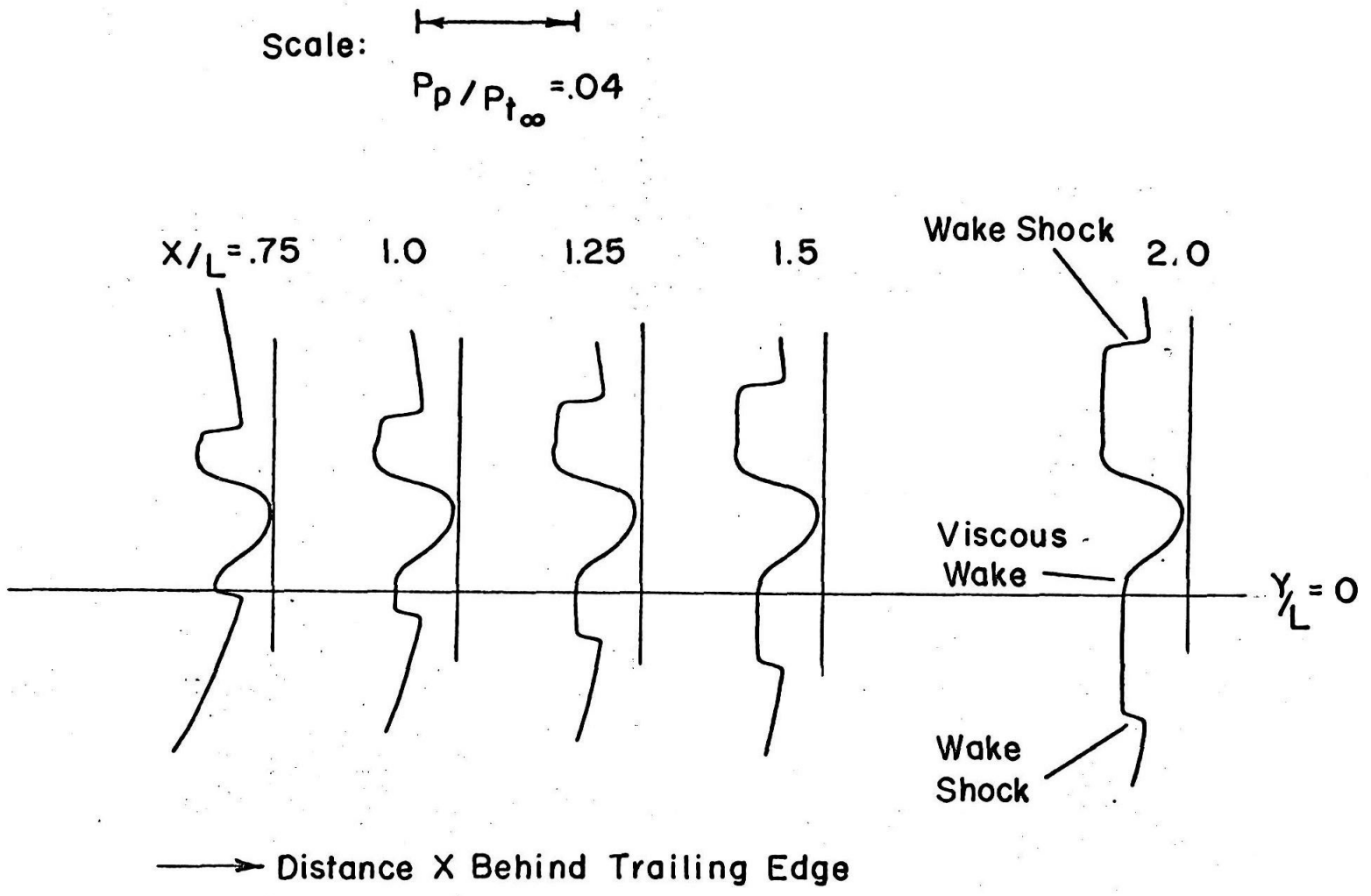

FIG. 11 b EXPERIMENTAL PITOT PRESSURE TRACE IN NEAR WAKE OF A FLAT PLATE AT AN ANGLE OF ATTACK
(Continuation Of Fig. 11a)

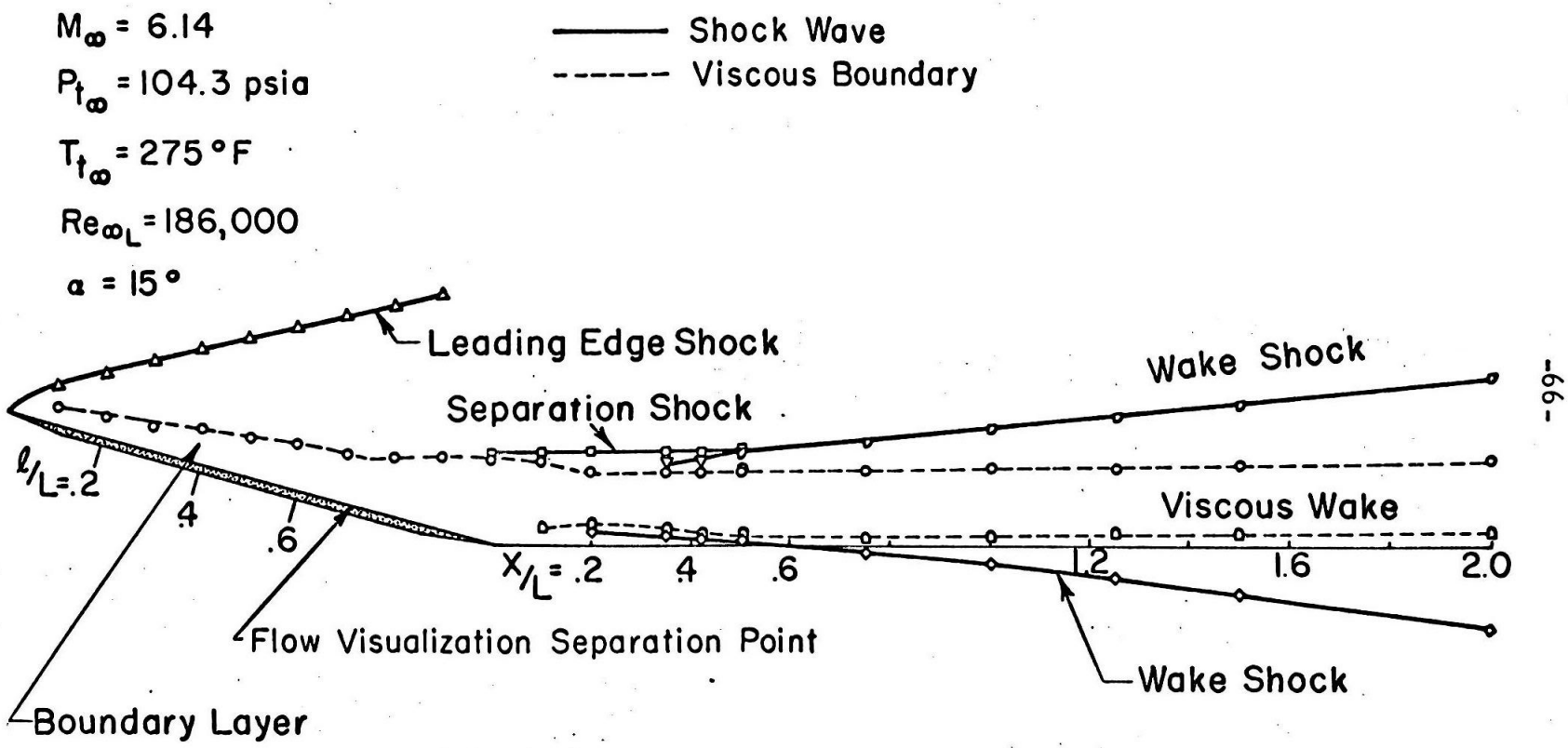

FIG. 12 MEASURED FLOW FIELD ABOUT FLAT PLATE AT ANGLE OF ATTACK

$M_\infty = 6.14$

$P_{t_\infty} = 104.3$ psia

$T_{t_\infty} = 275°F$

$Re_{\infty_L} = 186{,}000$

$\alpha = 22.5°$

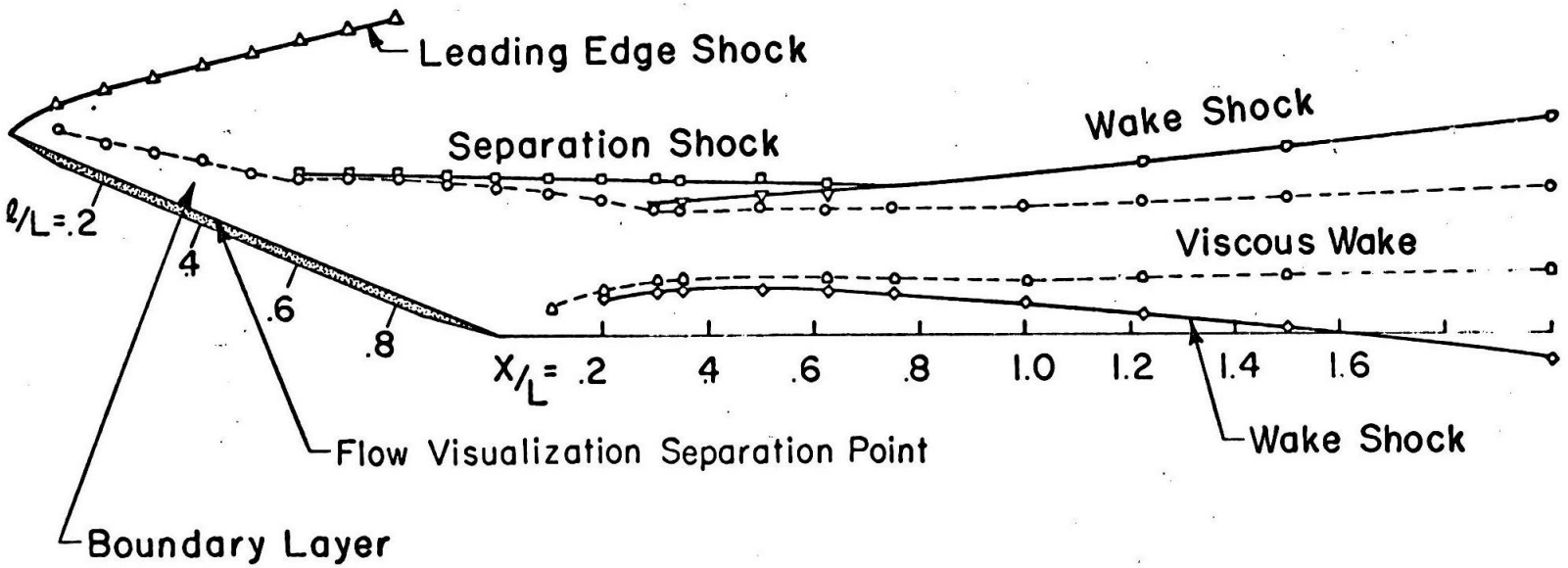

FIG. 13 MEASURED FLOW FIELD ABOUT FLAT PLATE AT ANGLE OF ATTACK

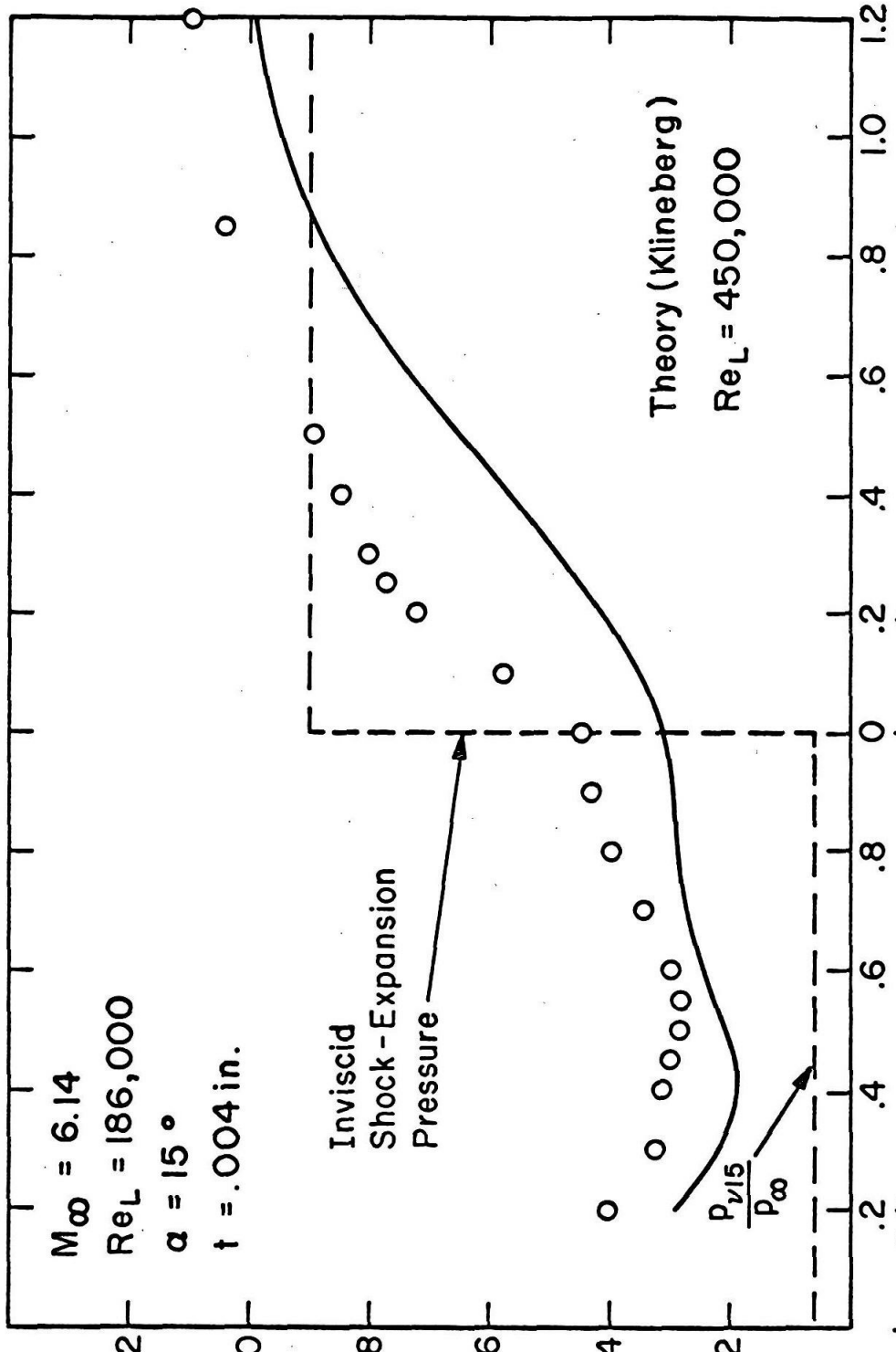

FIG. 14 PRESSURE DISTRIBUTION ON LEEWARD SIDE OF FLAT PLATE AND IN NEAR WAKE BEHIND PLATE AS COMPARED TO INVISCID PRESSURE CALCULATION AND KLINEBERG'S INTEGRAL THEORY

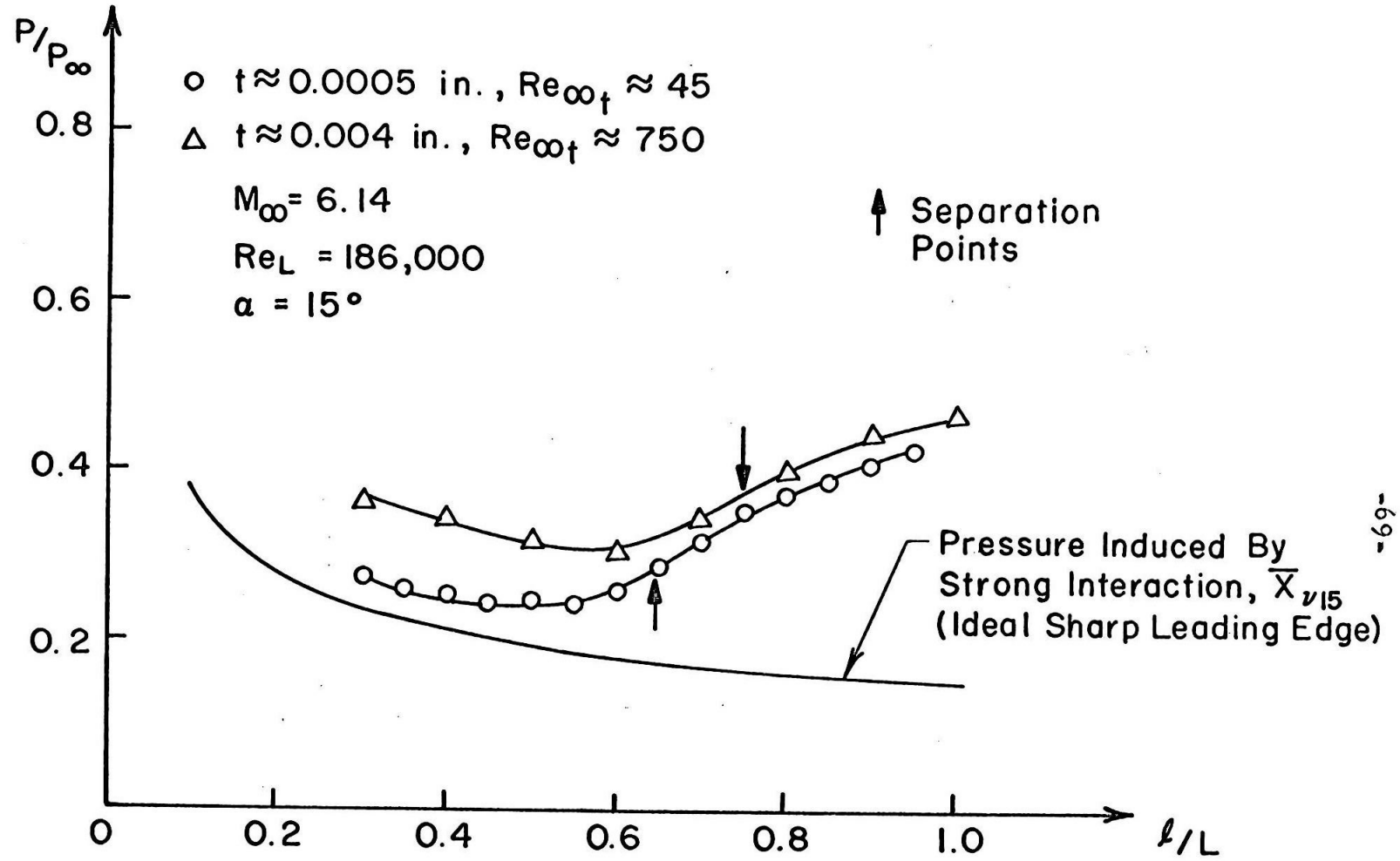

FIG. 15 LEEWARD SURFACE PRESSURE DISTRIBUTION FOR BLUNT AND SHARP PLATE COMPARED TO PRESSURE INDUCED BY VISCOUS-INVISCID INTERACTION BEHIND IDEALLY SHARP LEADING EDGE

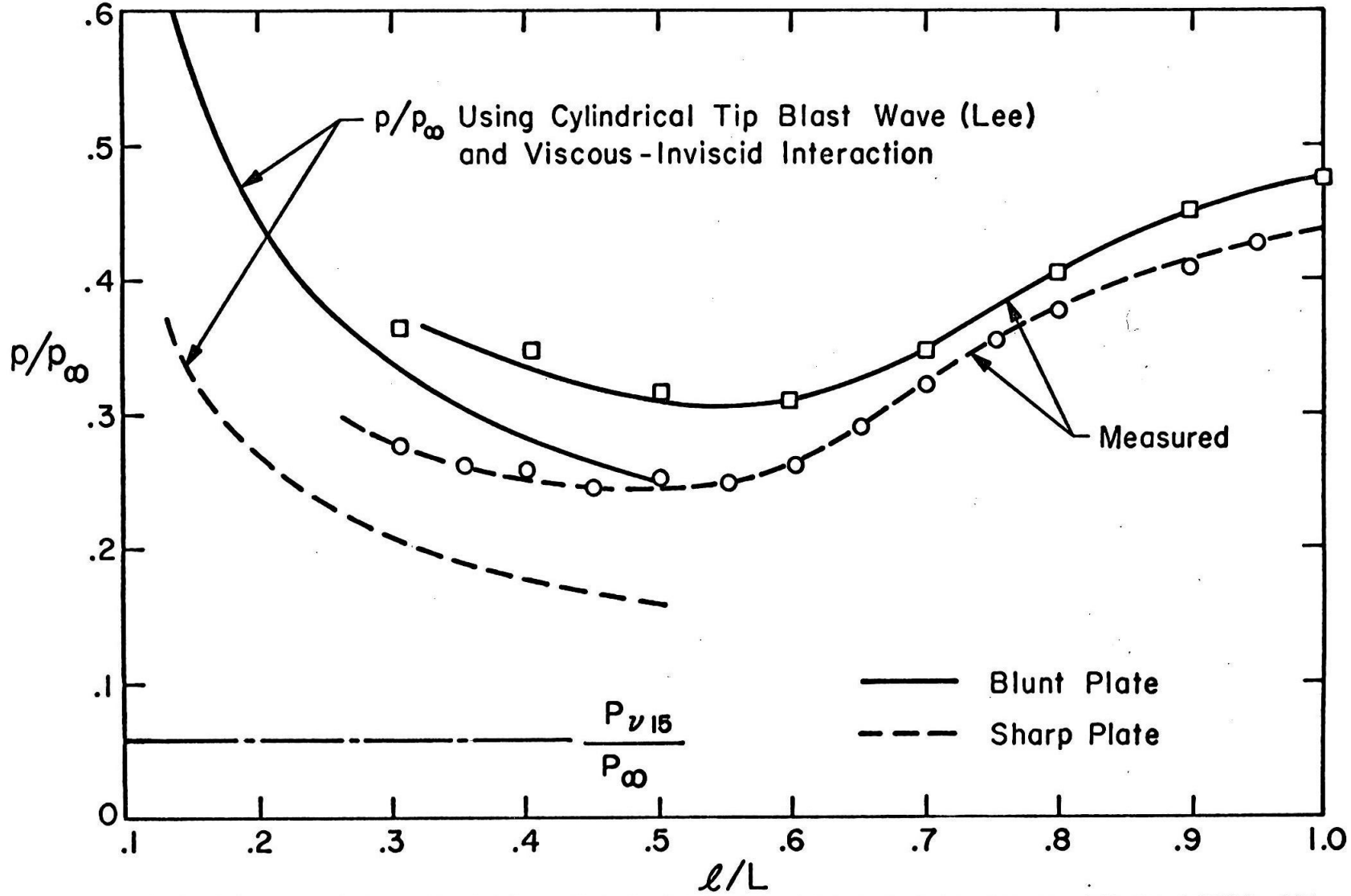

FIG. 16 PRESSURE DISTRIBUTIONS ON LEEWARD SURFACES OF FLAT PLATES AT $\alpha = 15°$ COMPARED TO A THEORETICAL CALCULATION FOR THE TWO CASES OF DIFFERENT NOSE-BLUNTNESS

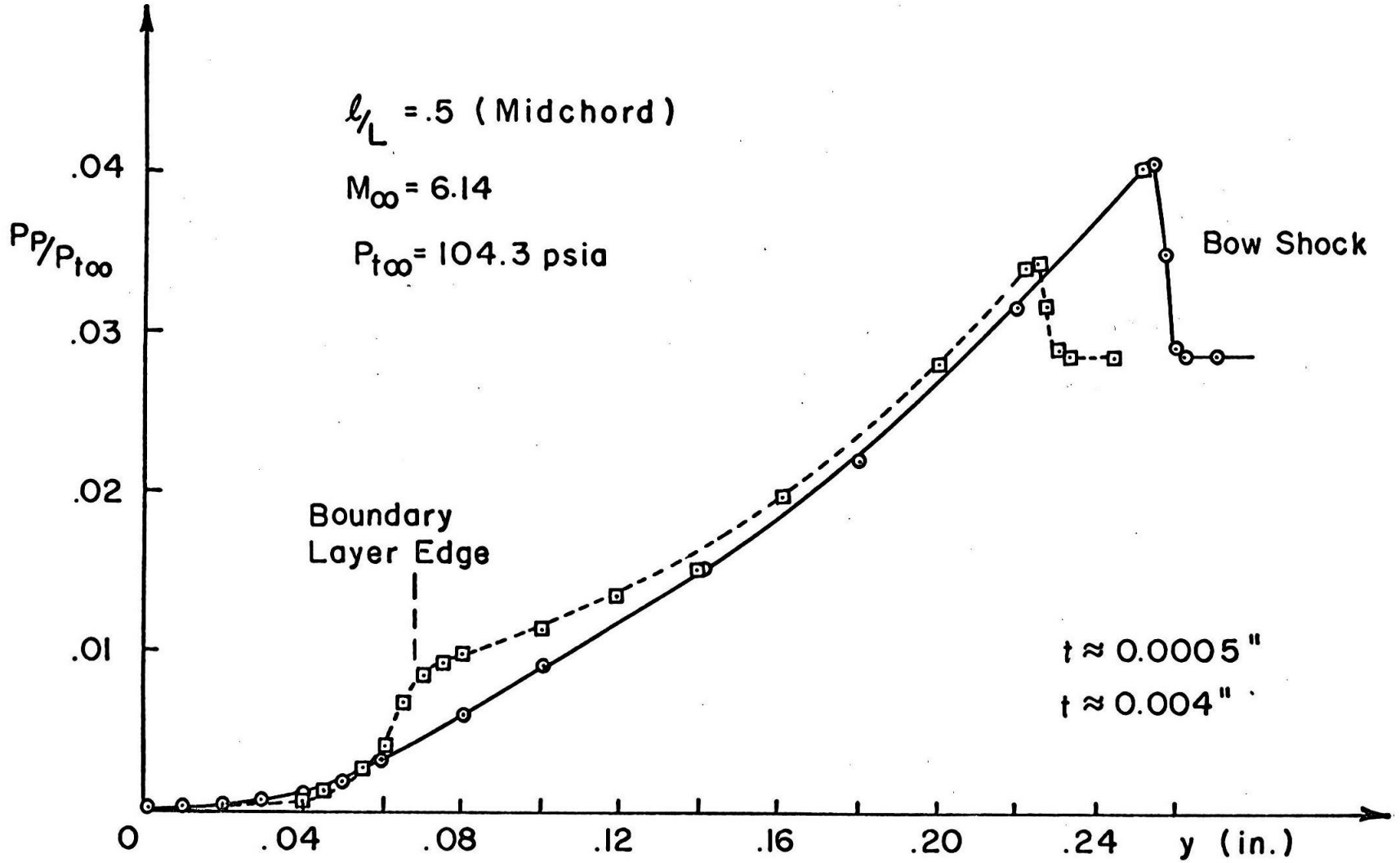

FIG. 17 TYPICAL PITOT PRESSURE PROFILE IN ATTACHED BOUNDARY LAYER OVER LEEWARD SURFACE OF SHARP AND BLUNT FLAT PLATE AT 15° INCIDENCE

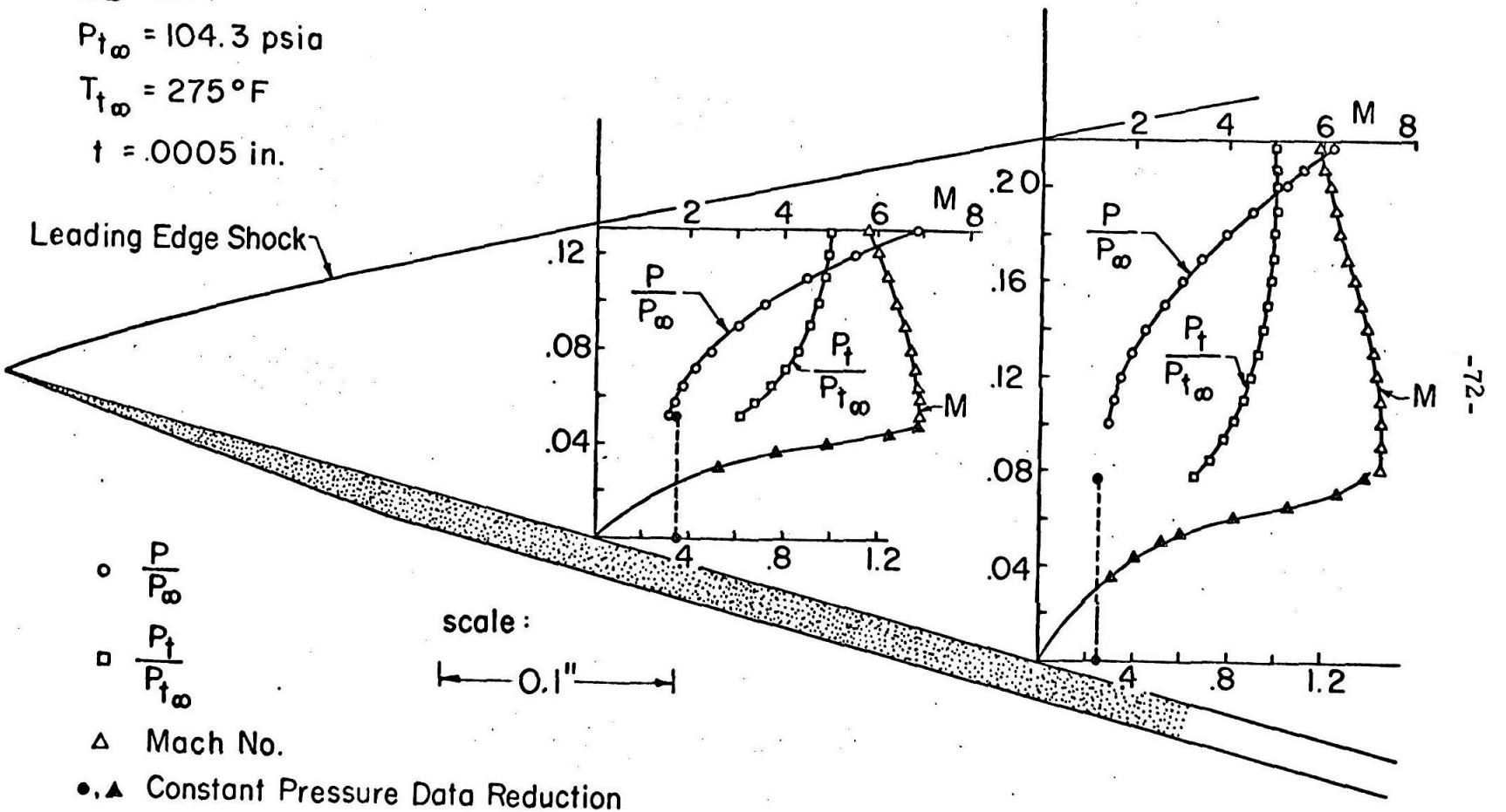

FIG.18a MEASURED FLOW PROFILES ON LEEWARD SIDE OF PLATE WITH "SHARP" LEADING EDGE

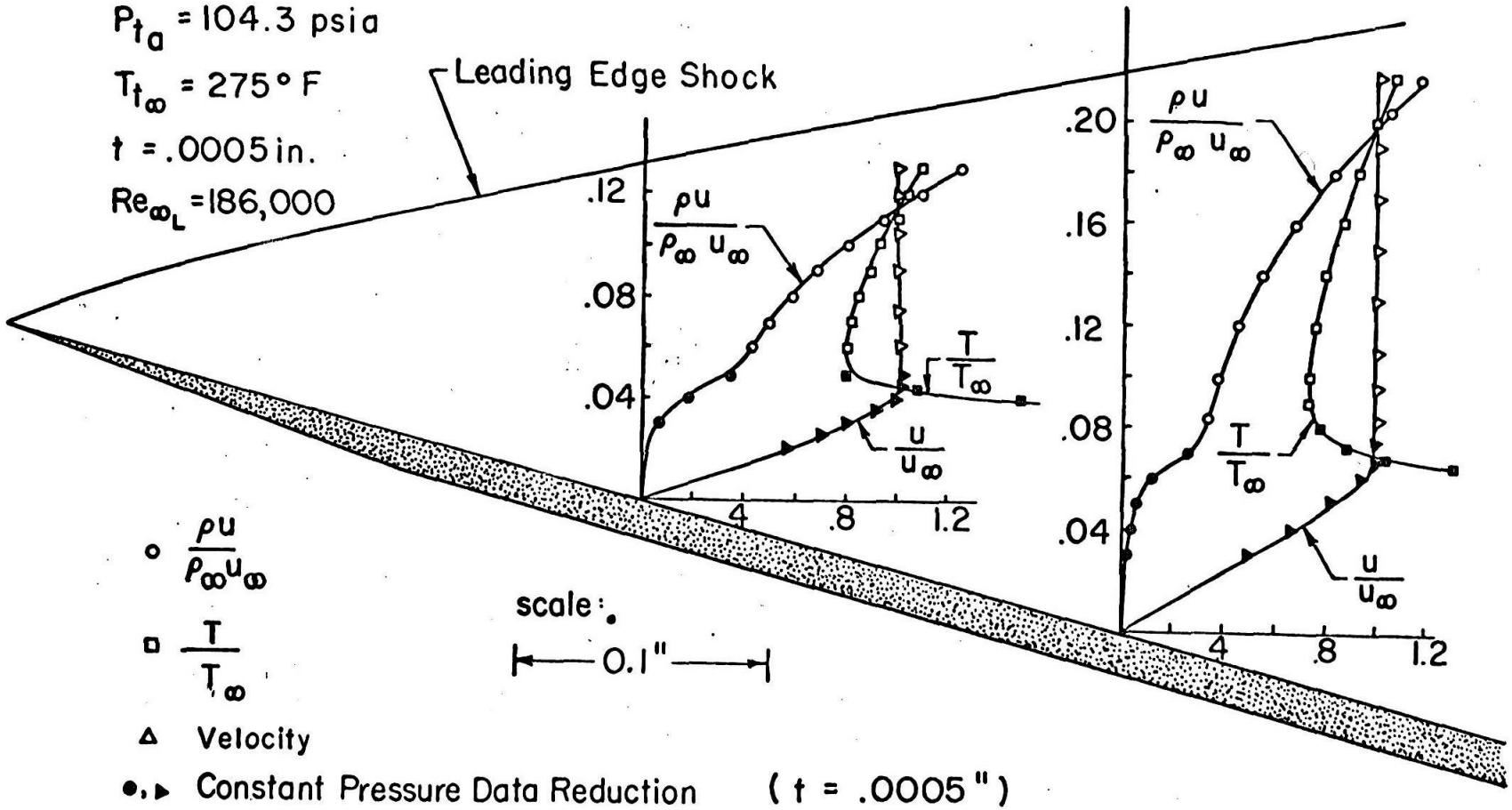

FIG.18b MEASURED FLOW PROFILES ON LEEWARD SIDE OF PLATE WITH "SHARP" LEADING EDGE

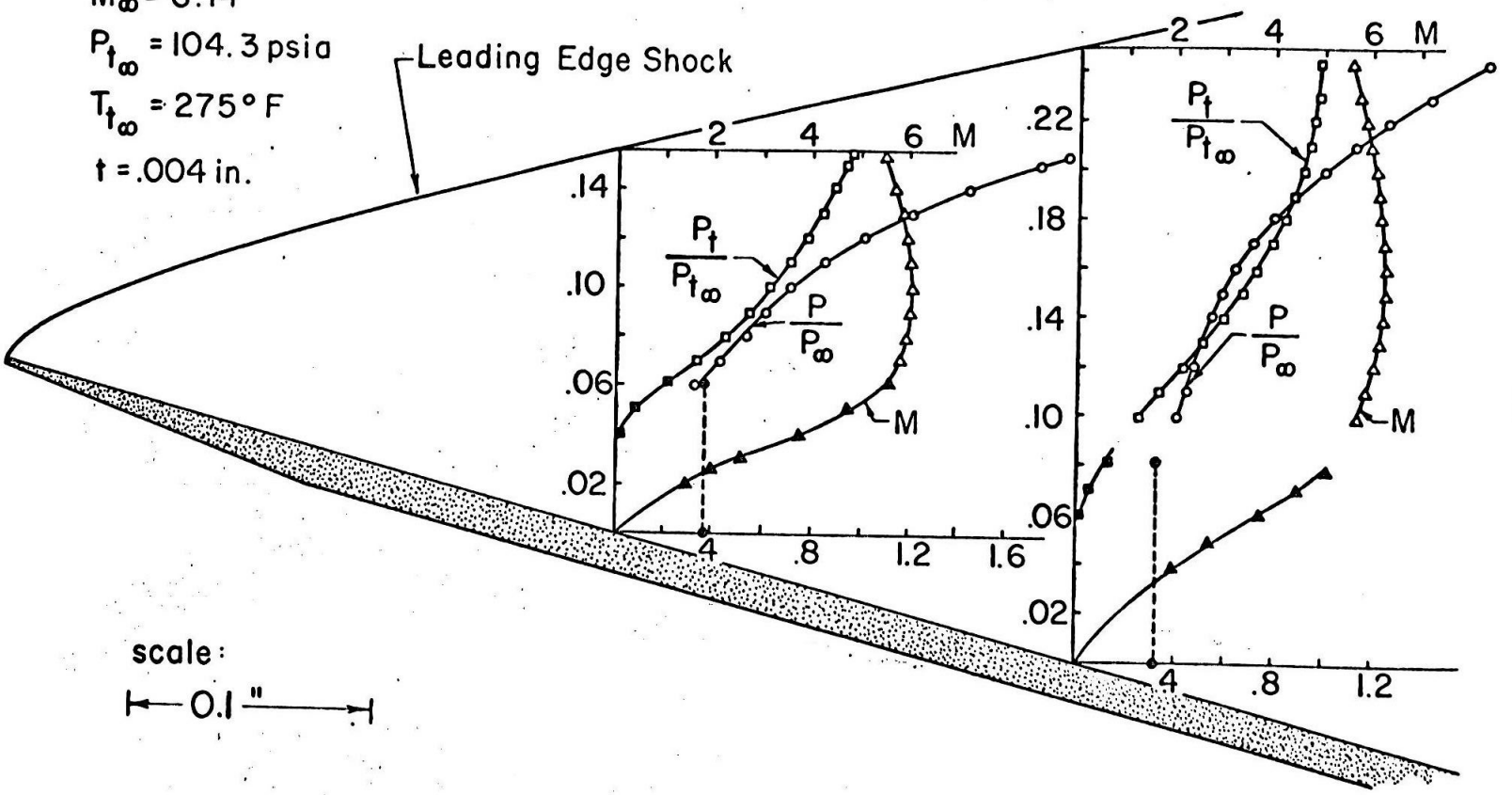

FIG. 19a MEASURED FLOW PROFILES ON LEEWARD SIDE OF PLATE WITH "BLUNT" LEADING EDGE (t = .004")

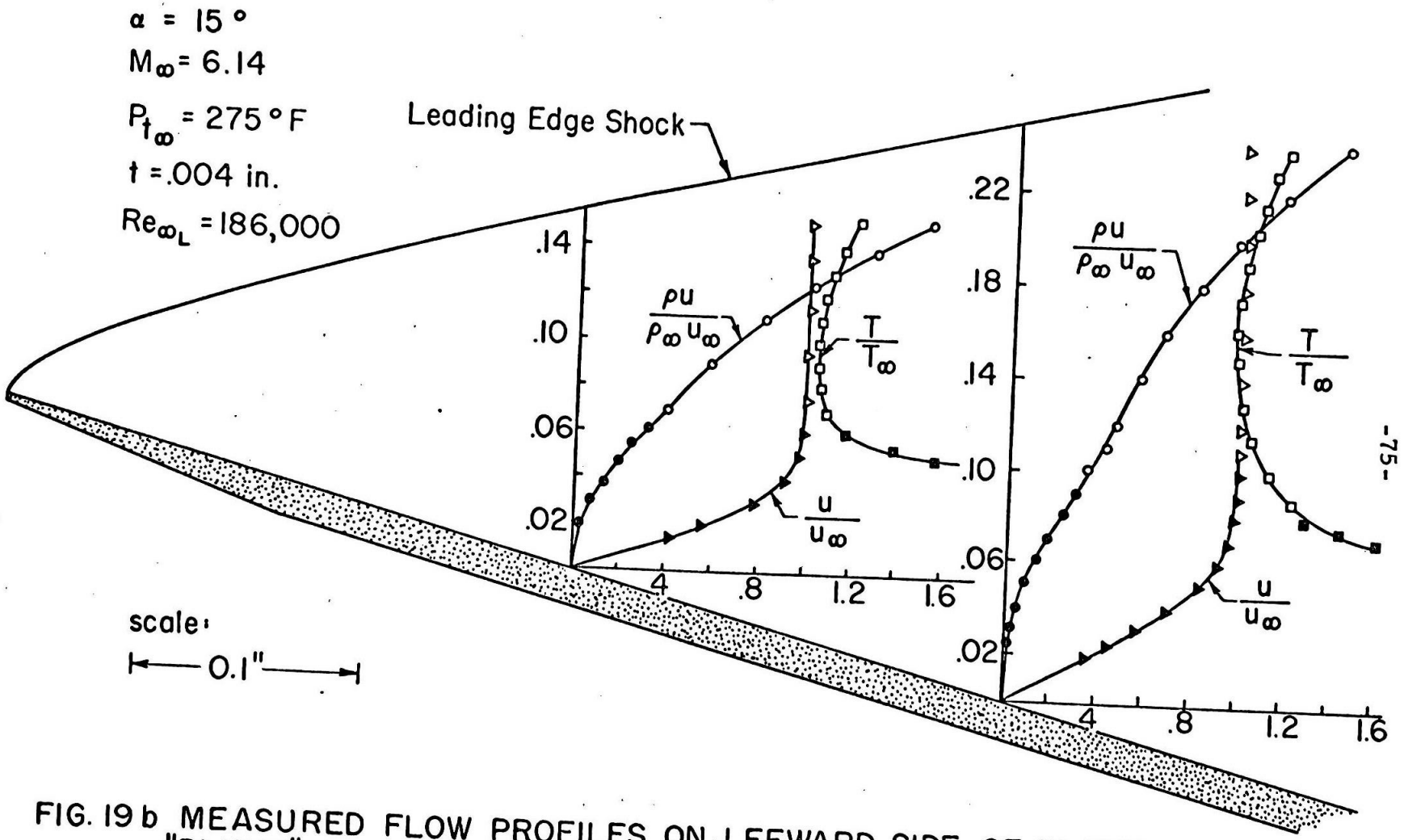

FIG. 19b MEASURED FLOW PROFILES ON LEEWARD SIDE OF PLATE WITH "BLUNT" LEADING EDGE (t = .004")

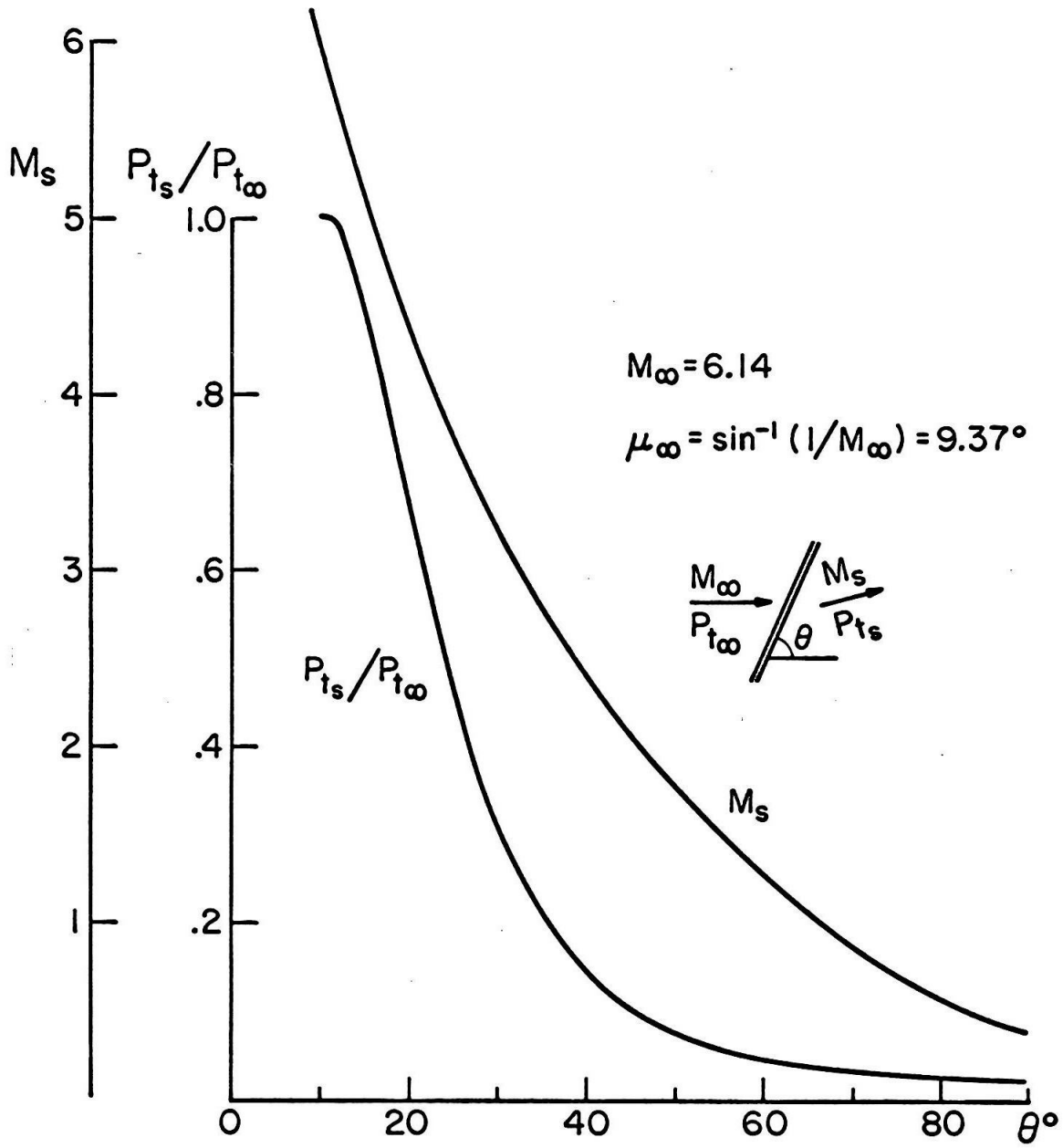

FIG.20 MACH NUMBER AND TOTAL PRESSURE ACROSS OBLIQUE SHOCK AS FUNCTION OF SHOCK INCLINATION

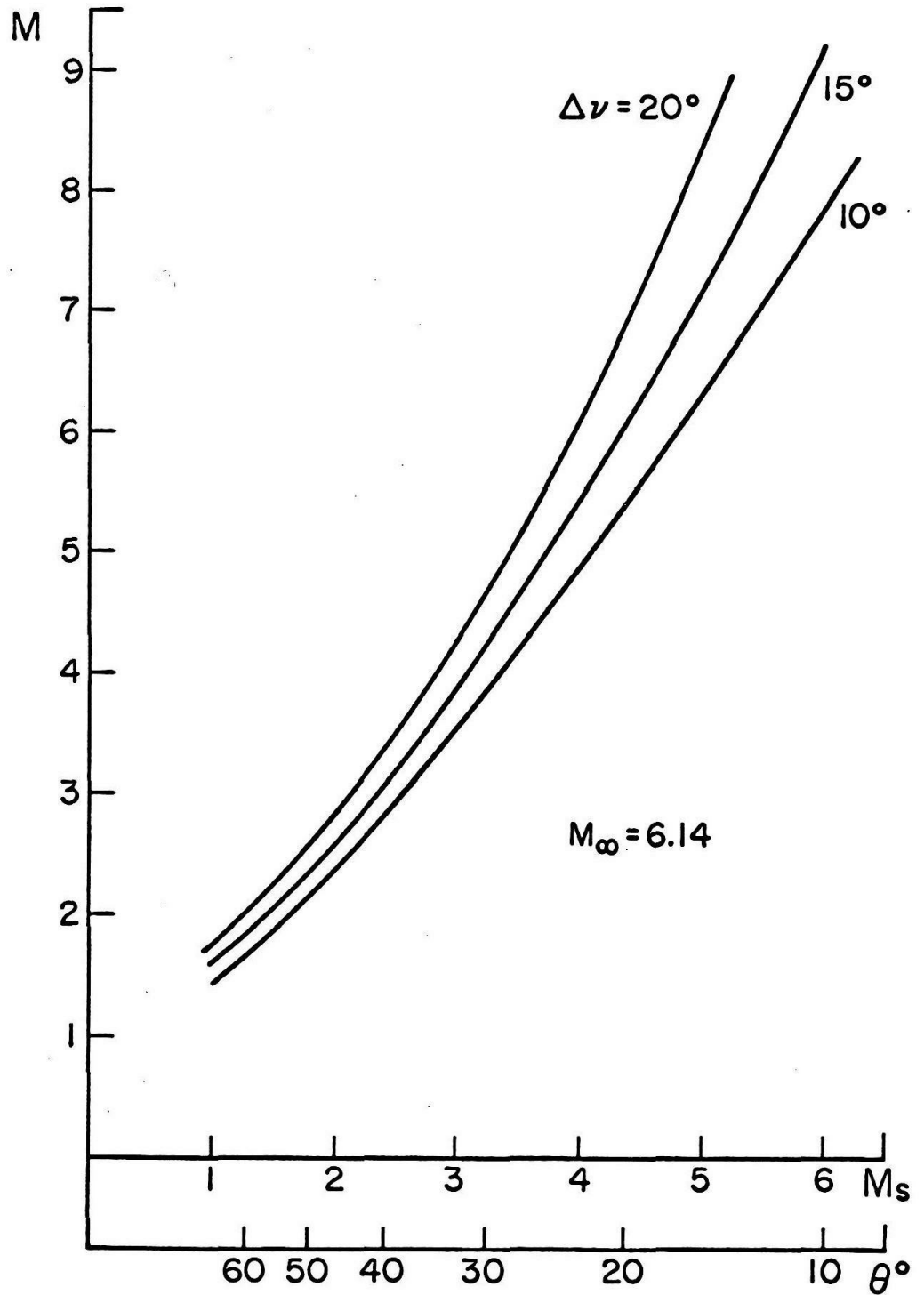

FIG. 21 MACH NUMBER OF PARTICLE AFTER COMPRESSION IN OBLIQUE SHOCK FOLLOWED BY EXPANSION $\Delta\nu$

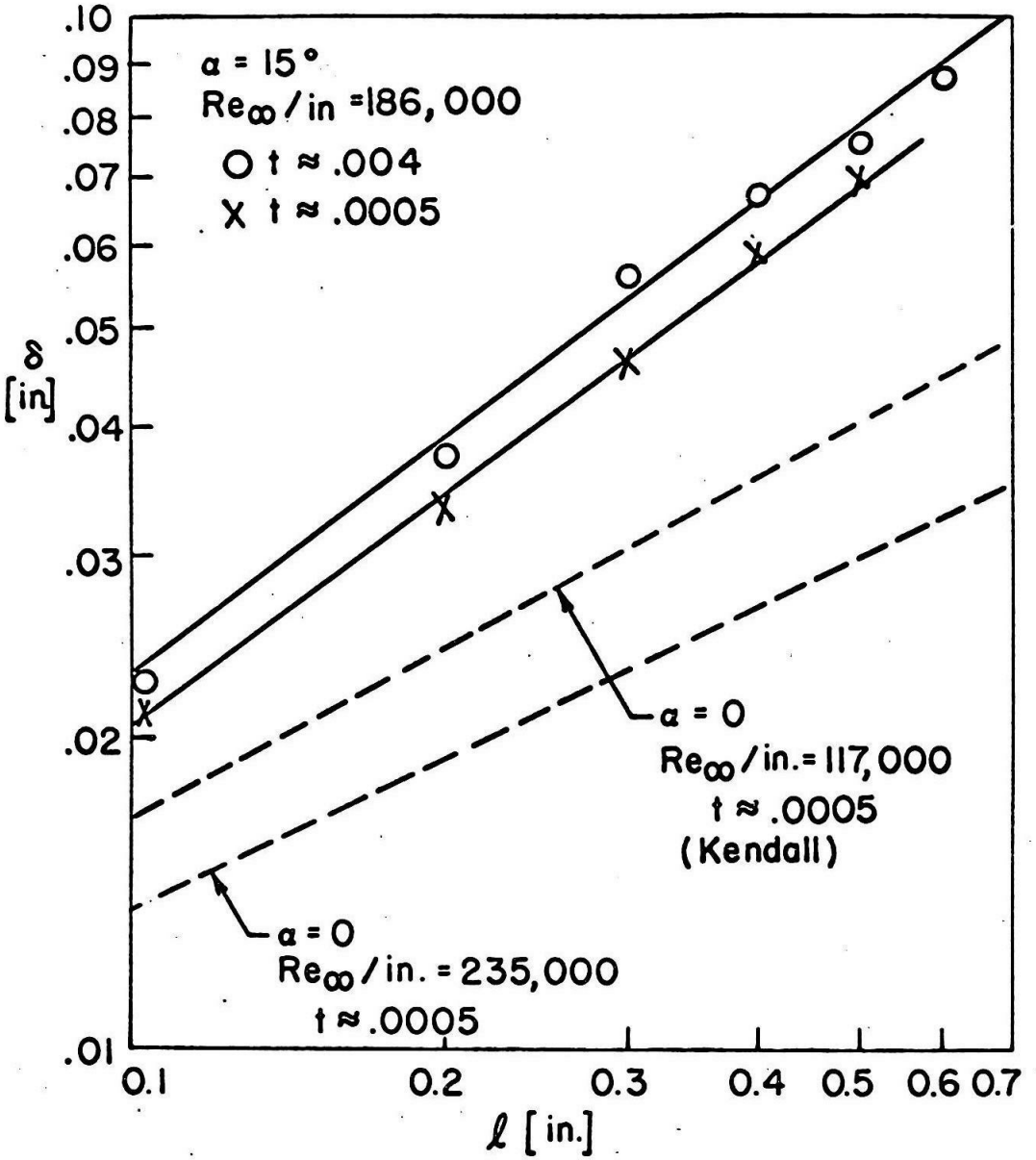

FIG. 22 BOUNDARY LAYER THICKNESS OVER SHARP AND BLUNT FLAT PLATE AT AN INCIDENCE WITH $M_\infty = 6.14$

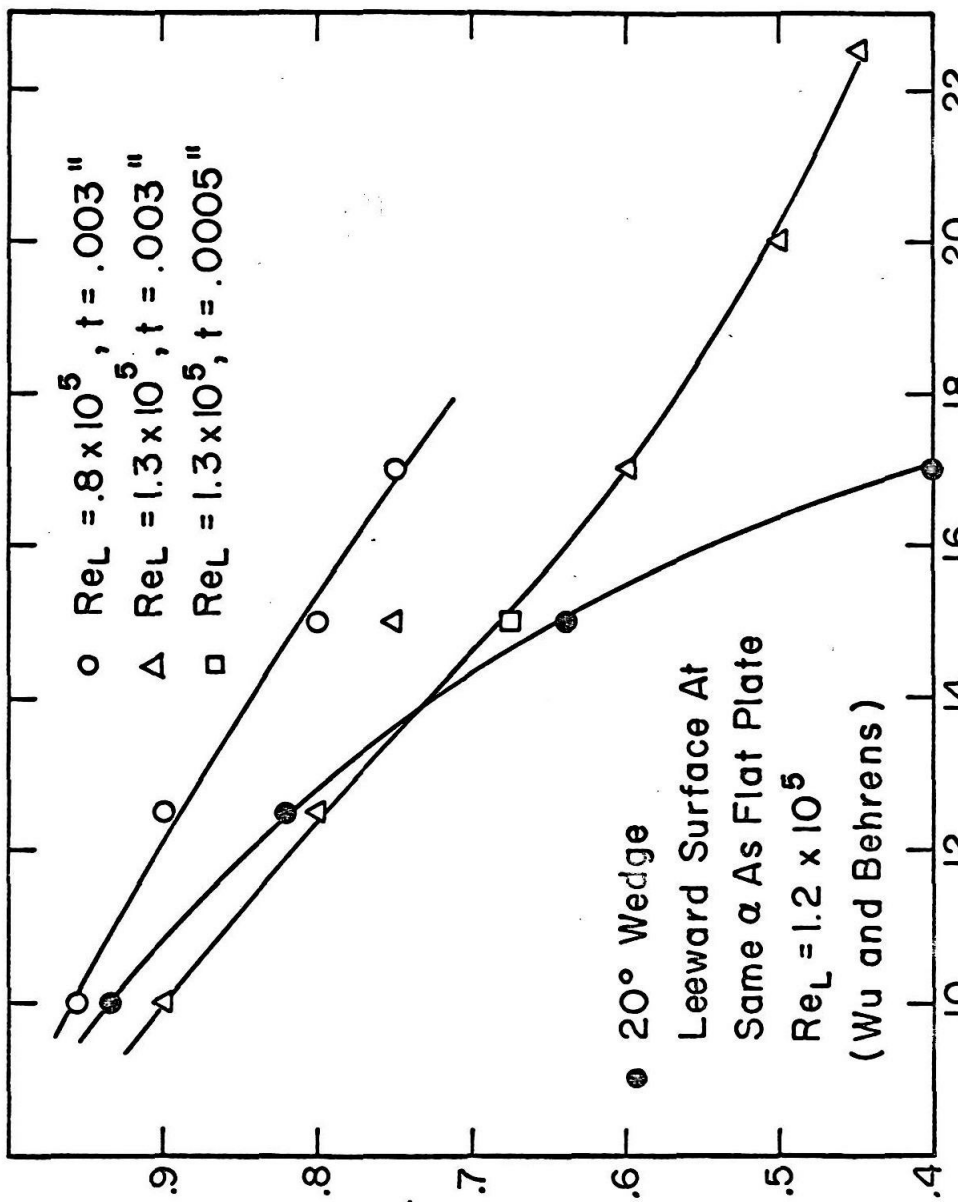

FIG. 23 BOUNDARY LAYER SEPARATION POINT LOCATION ON LEEWARD SURFACE OF FLAT PLATE AND 20° WEDGE

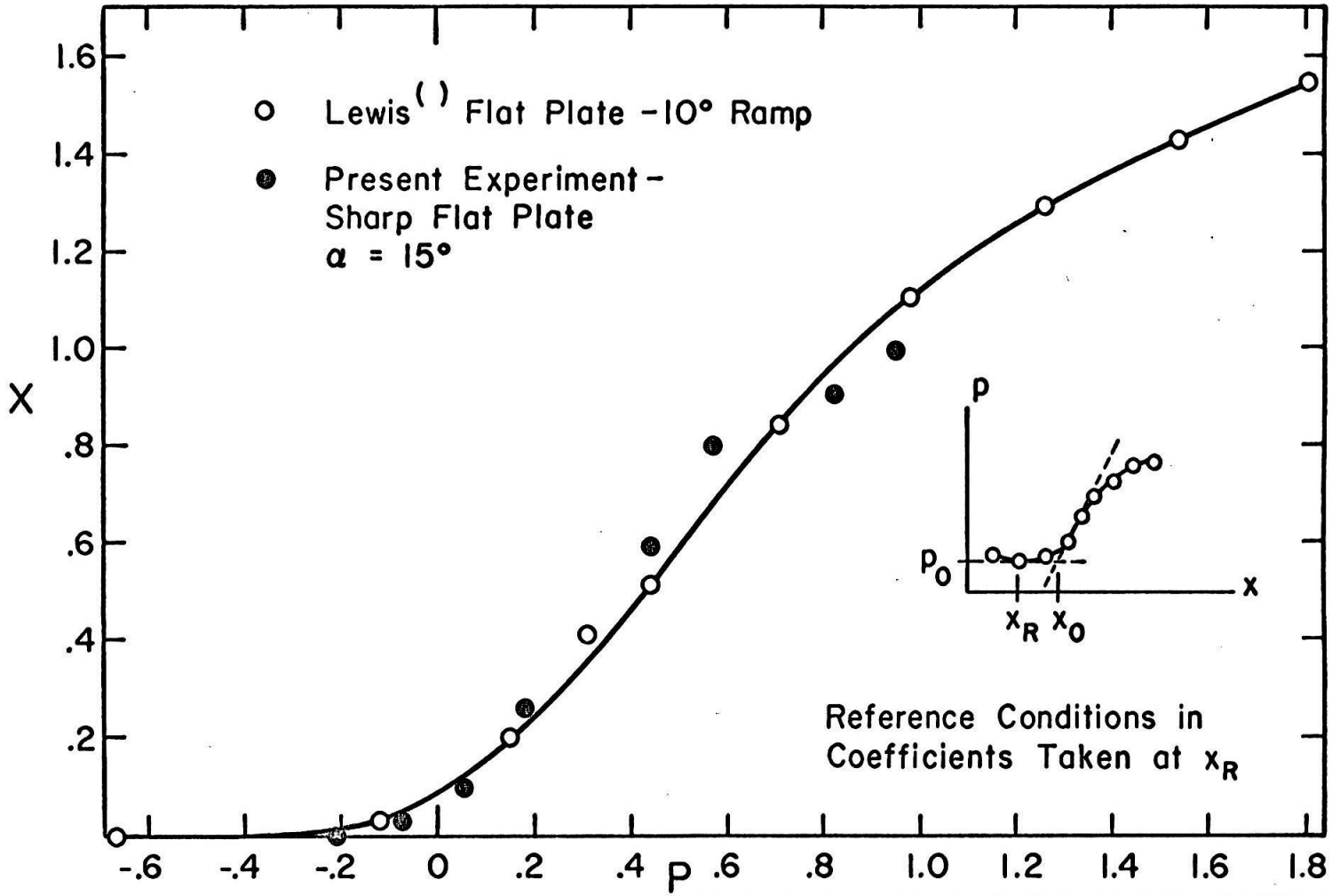

FIG. 24 CHAPMAN FREE INTERACTION PRESSURE CORRELATION ON LEEWARD SIDE OF FLAT PLATE (α=15°) COMPARED WITH FLAT PLATE - 10° RAMP CONFIGURATION

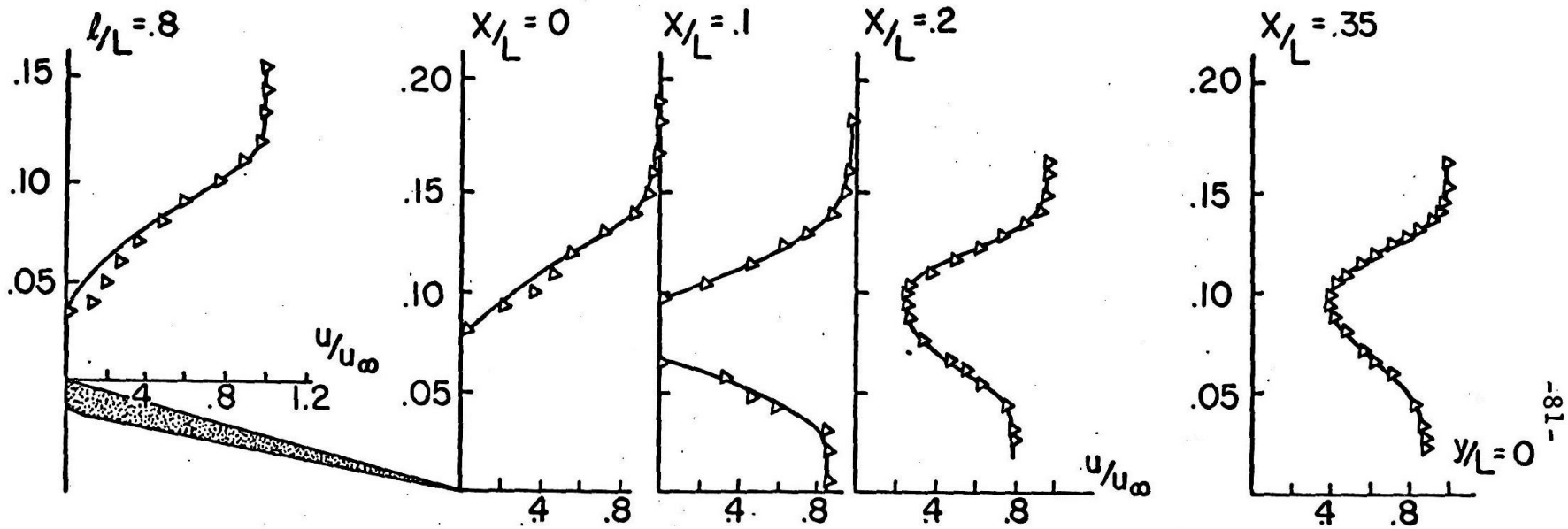

$\alpha = 15°$ $\quad Re_{\infty_L} = 186{,}000$

$M_\infty = 6.14$

$P_{t_\infty} = 104.3$ psi

$T_{t_\infty} = 275°F$

$t = .003$ in.

FIG. 25 VELOCITY PROFILES IN SEPARATED FLOW REGION AND IN NEAR WAKE OF FLAT PLATE AT $\alpha = 15°$

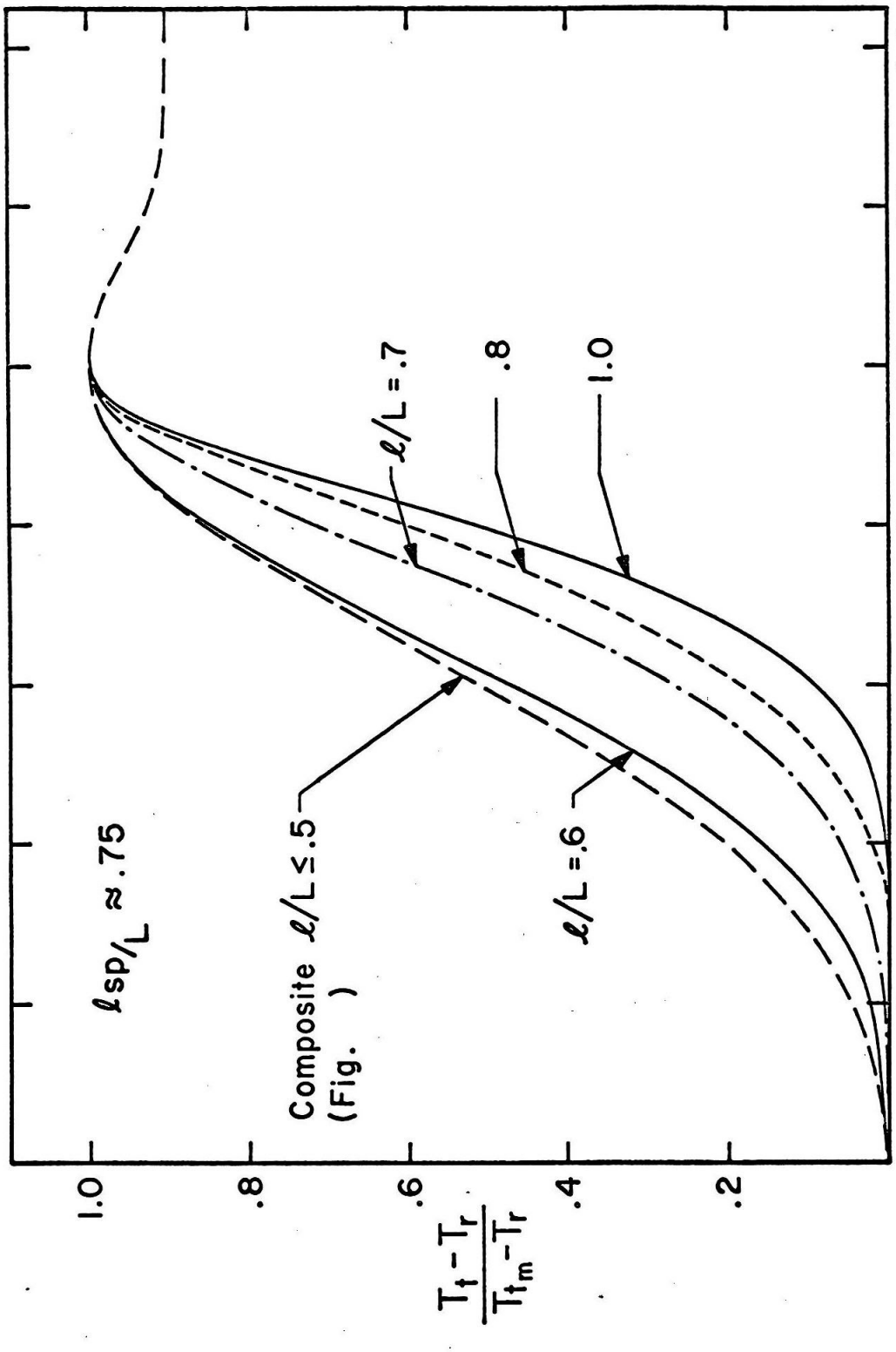

FIG. 26 NORMALIZED TOTAL TEMPERATURES IN SEPARATION REGION

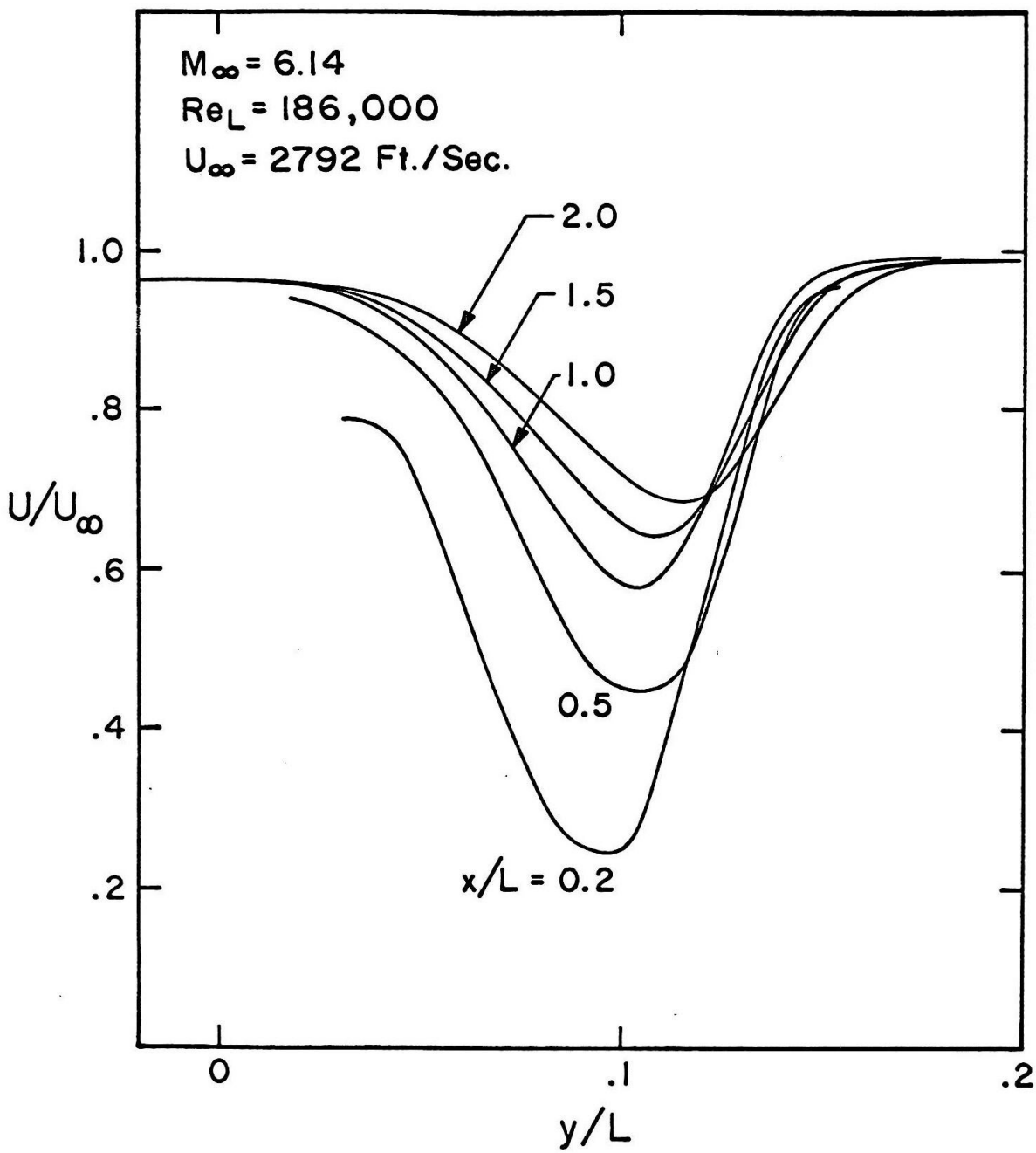

FIG. 27 VELOCITY PROFILES WITHIN VISCOUS WAKE BEHIND FLAT PLATE AT $\alpha = 15°$

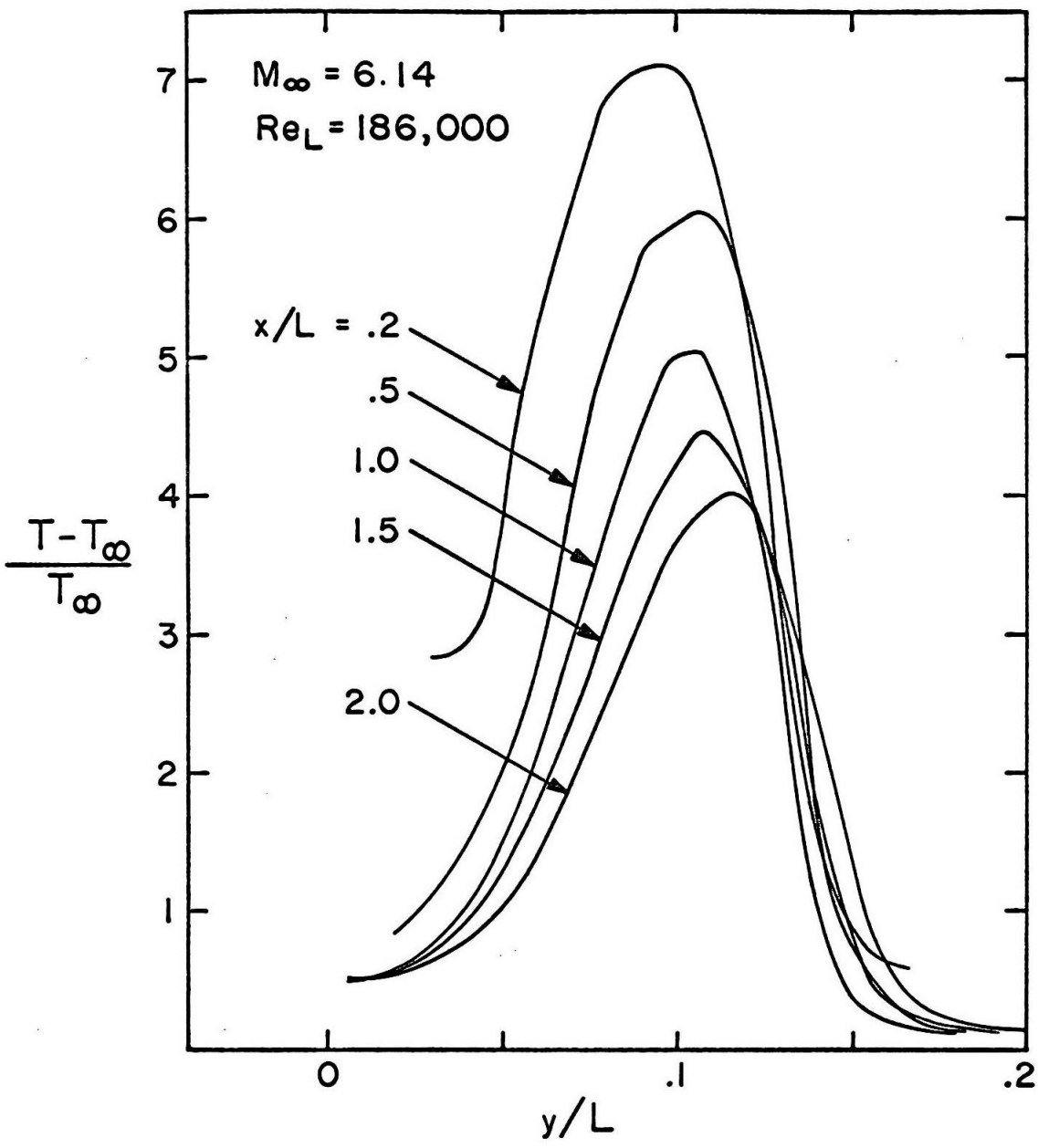

FIG. 28 TEMPERATURE EXCESS IN VISCOUS WAKE BEHIND FLAT PLATE AT $\alpha = 15°$

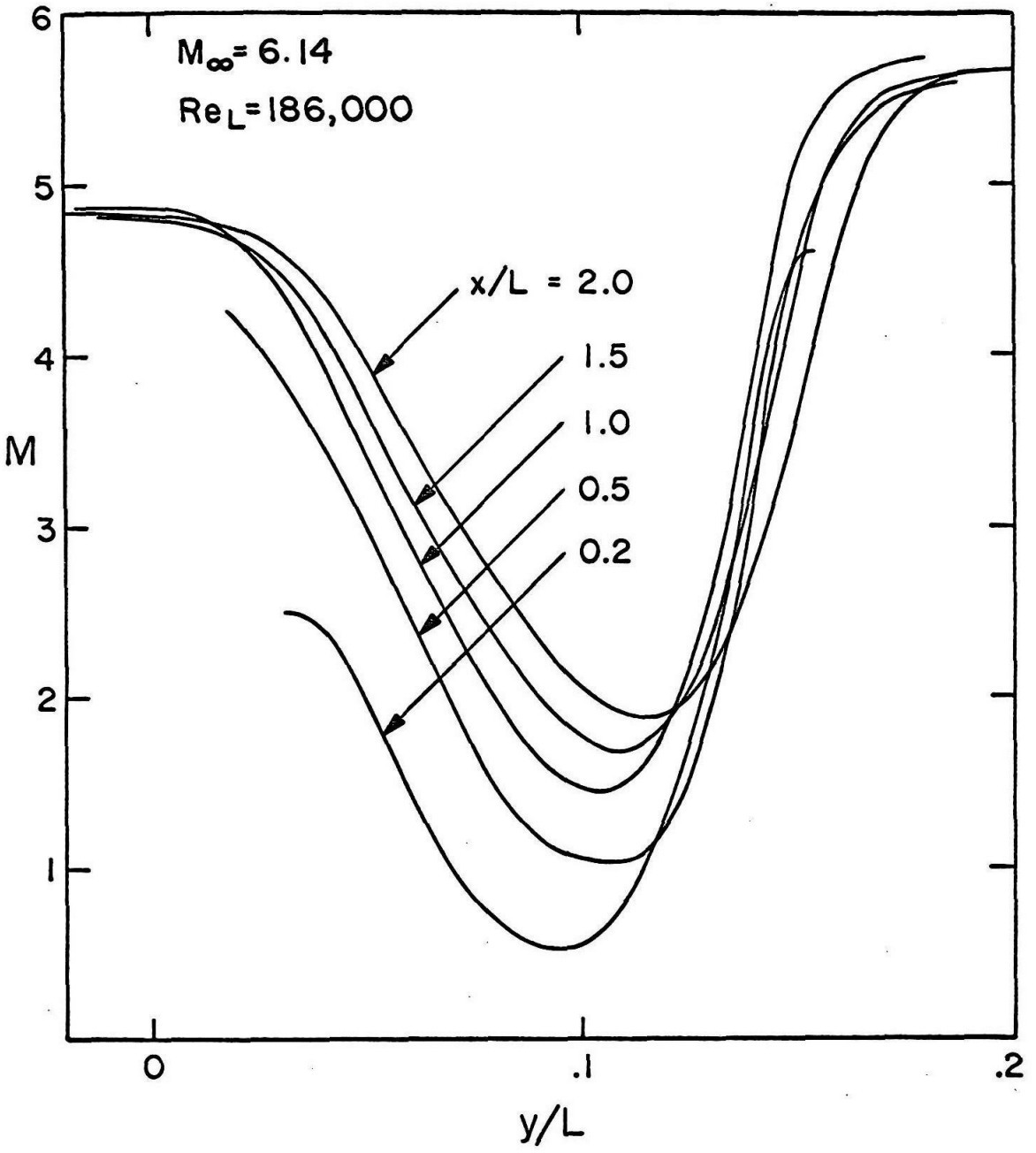

FIG. 29 MACH NUMBER DISTRIBUTION IN VISCOUS WAKE BEHIND FLAT PLATE AT $\alpha = 15°$

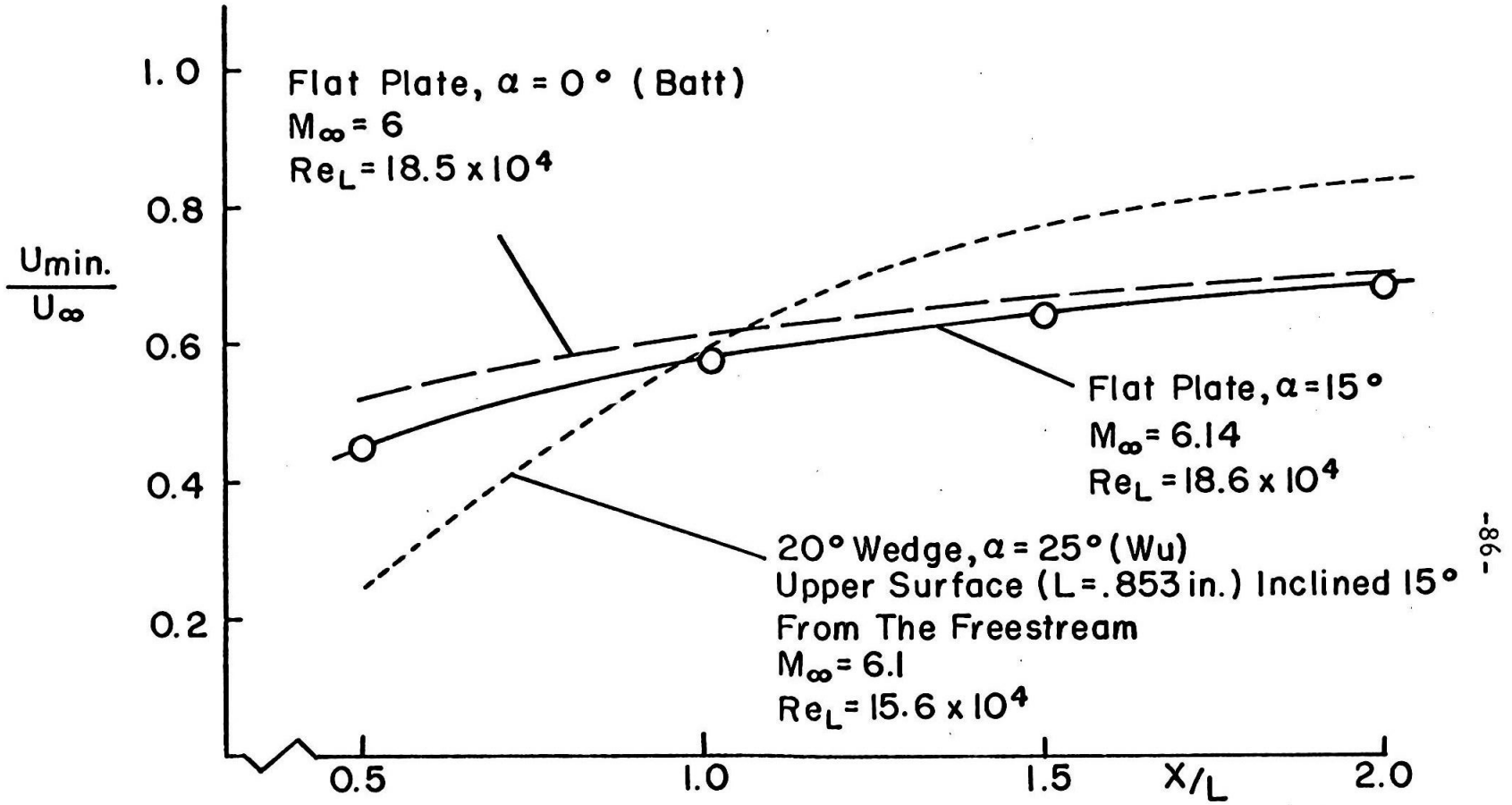

FIG. 30 MINIMUM VELOCITY IN WAKE OF FLAT PLATE AT ANGLE OF ATTACK COMPARED TO WEDGE AT ANGLE OF ATTACK AND THIN FLAT PLATE ALIGNED WITH FREESTREAM

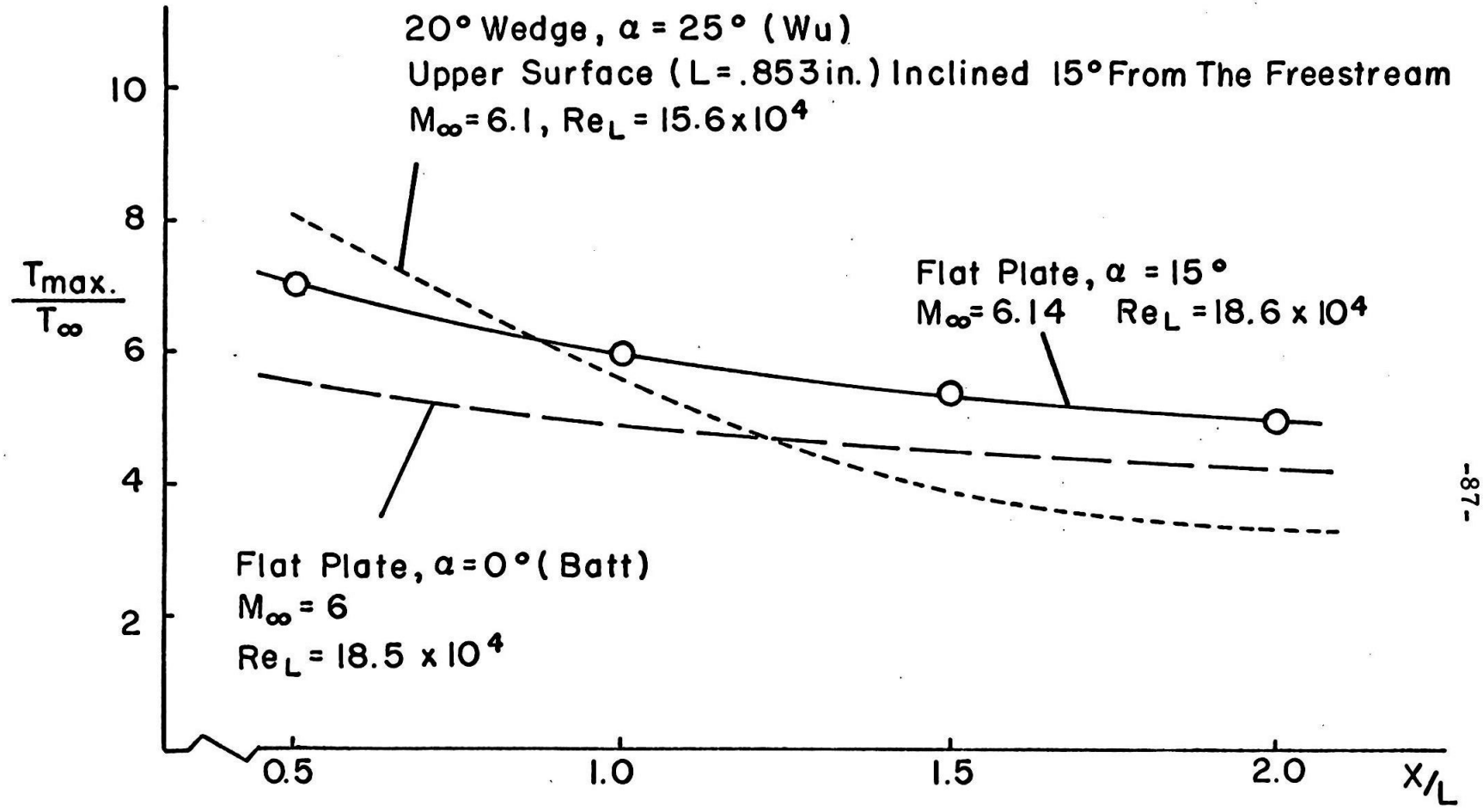

FIG. 31 MAXIMUM TEMPERATURE IN WAKE OF FLAT PLATE AT ANGLE OF ATTACK COMPARED TO WEDGE AT ANGLE OF ATTACK AND THIN FLAT PLATE ALIGNED WITH THE FREESTREAM

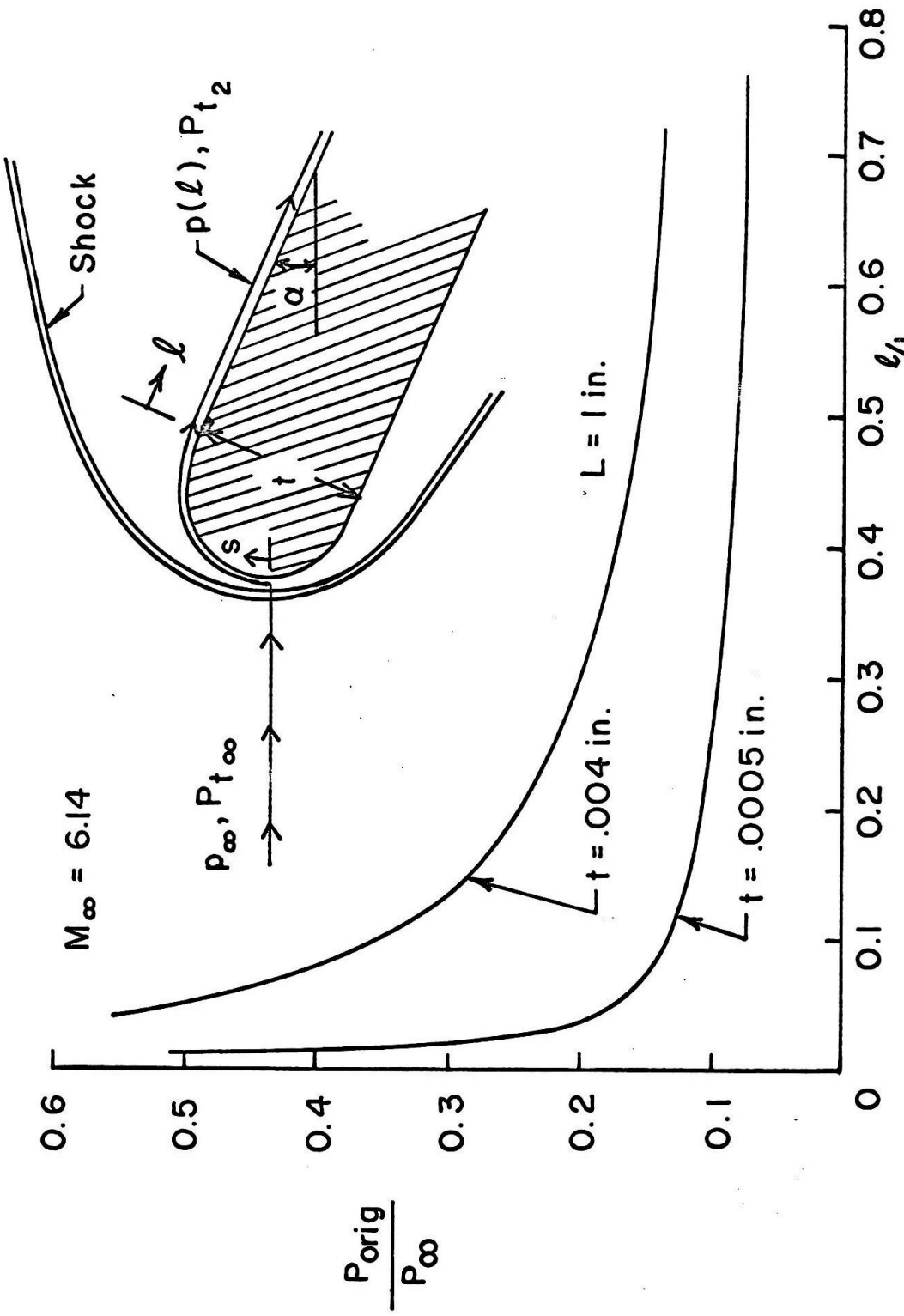

FIG. A-1 PRESSURE INDUCED ON INVISCID FLOW ABOUT LEEWARD SURFACE WITH HEMI-CYLINDRICAL TIP

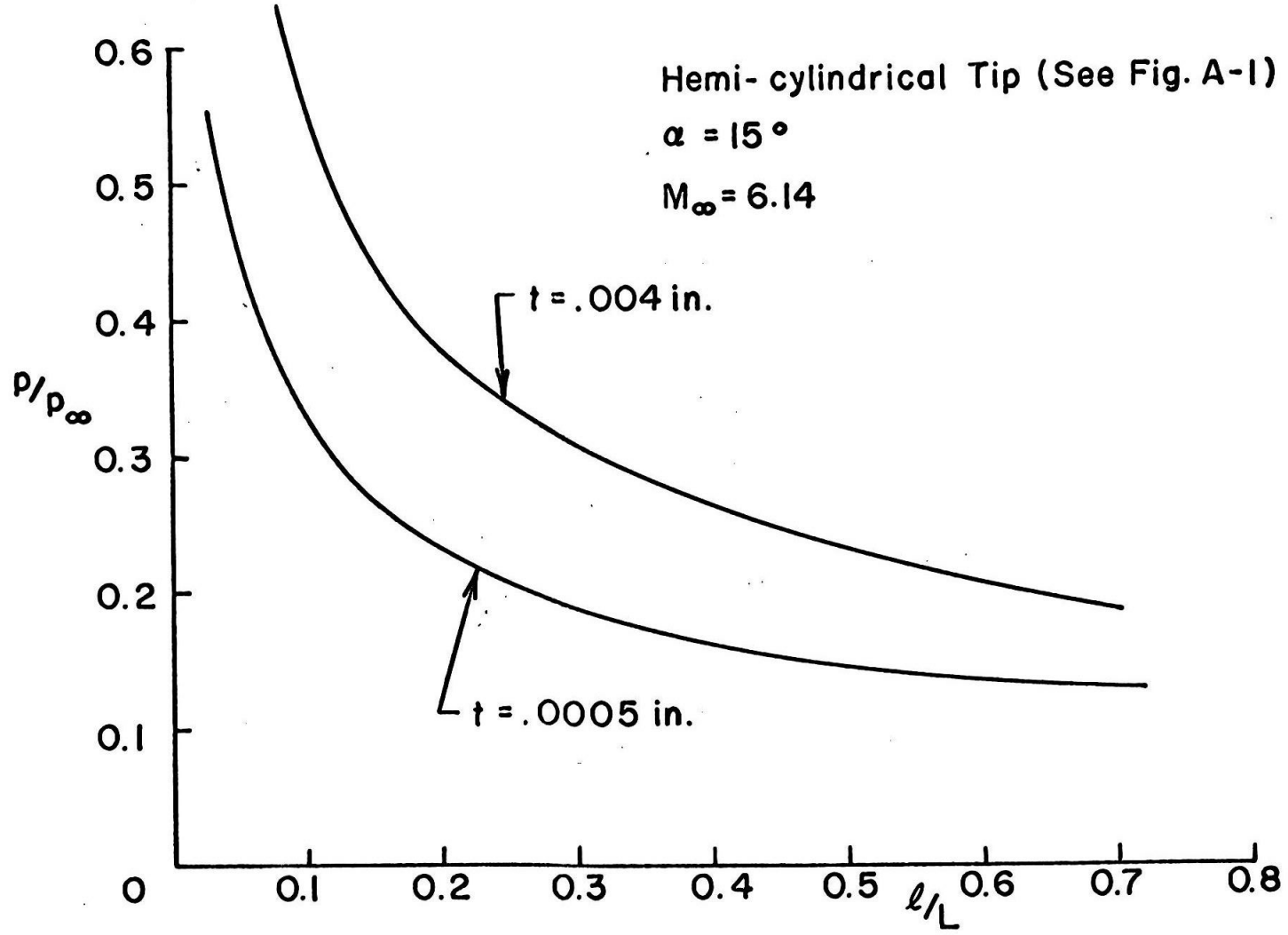

FIG. A-2 PRESSURE INDUCED BY EFFECTS OF BLUNT TIP AND LOCAL VISCOUS-INVISCID INTERACTION